

7C02246



TDI LIBRARY SERVICES

11340
Olympic Blvd.
Suite 355
Los Angeles
California
90064-1639
P (310) 268-0601
F (310) 268-0701
tdi@tdico.com

BILL TO

Ut-Battelle
Bldg. 4500N, MS-6193
PO Box 2008
Oak Ridge, TN 37831-6193
USA

SHIP TO

James Kidder
Ut-Battelle

Date Rec'd

03/02/2007

Need By

[Empty box]

Ordered By

[Empty box]

P (865) 574-1241

F (865) 574-1240

Requestor

James Kidder

Client Number

52714X

Service & Delivery

REGULAR FedEx

Journal/Book Title

Journal of Geophysical Research-Atmospheres

Author 1

Dan L

Author 2

Ji J

Month	Year	Volume	Issue	Pages
	2007	112		1-18

Article Title

Use of ISLSCP II data to intercompare and validate the terrestrial net primary production in a land.

Order Special Instructions

MC: 4500N 6191

Use of ISLSCP II data to intercompare and validate the terrestrial net primary production in a land surface model coupled to a general circulation model

Li Dan,¹ Jinjun Ji,¹ and Yong He²

Received 30 June 2006; revised 2 November 2006; accepted 10 November 2006; published 24 January 2007.

[1] Using the global terrestrial NPP and climate data from International Satellite Land Surface Climatology Project Initiative II (ISLSCP II) and additional NPP data, we validated the NPP simulations and explored the relationship between NPP and climate variation in a global two-way coupled model AVIM-GOALS. The strength of this study is that the global simulations produced will enhance interactive climate and vegetation study; however, the weakness is that the NPP distribution is not fully reproduced in some regions, because of the coarse model resolution and climate biases. Global NPP is spatially consistent with IGBP NPP and MODIS data, though there is a discrepancy in NPP (significantly lower values) for boreal forests and tundra, due to the underestimated temperature. The NPP distribution in China indicates agreement with IGBP data, but the IGBP data in northeast China (around 48°N) seem to be slightly high in contrast with other modeled and estimated NPP. The spatial structure of NPP in USA and Australia roughly corresponds to the IGBP NPP data and GPPDI Gridded data, and a possible lower value of GPPDI data in central Australia exists, in contrast with other NPP data. The globally averaged NPP of 447.47 g C m⁻² year⁻¹ is close to the 450.42 g C m⁻² year⁻¹ from IGBP data. The global relative error of simulated NPP against IGBP data is about 20% and is comparable to other global biogeochemical models. The meridional variation of globally zonal mean NPP corresponds more to the meridional change of precipitation than temperature. The global NPP for all vegetation types is highly statistically significant in correlation with precipitation.

Citation: Dan, L., J. Ji, and Y. He (2007), Use of ISLSCP II data to intercompare and validate the terrestrial net primary production in a land surface model coupled to a general circulation model, *J. Geophys. Res.*, 112, D02S90, doi:10.1029/2006JD007721.

1. Introduction

[2] Net primary production (NPP) is an important variable for global carbon cycle and the feedback between terrestrial ecosystems and atmosphere, and many studies have addressed the view [Ciais *et al.*, 1995; Cramer *et al.*, 1999; Ruimy *et al.*, 1999; Running *et al.*, 1999; Nemani *et al.*, 2003; Williams *et al.*, 2005]. NPP integrates climatic, ecological, geochemical, and human influences on the biosphere [Nemani *et al.*, 2003]. NPP is the difference between total photosynthesis (Gross Primary Production, GPP) and total plant respiration in an ecosystem [Clark *et al.*, 2001]. The process regulating NPP at regional to global scales can only be addressed with observational studies and models [Williams *et al.*, 2005], and modeling is required when measurements cannot provide a complete view of

biospheric biogeochemical activity [Running *et al.*, 1999]. There have been many biogeochemical models designed to simulate NPP, so the observed or field data are needed to calibrate and validate the models. Scurlock *et al.* [1999] also cited the importance of obtaining high-quality data of NPP from around the globe for comparing various models. Terrestrial NPP data are more widely available than other estimates of biosphere-atmosphere exchanges of carbon such as GPP and net ecosystem exchange (NEE), but there are significant problems with inconsistency in measurement techniques between NPP studies separated in space and time [Scurlock and Olson, 2002]. As a result, although there are many site-level or point NPP field measurements, the data cannot be used as direct validation of NPP simulations at regional or global scale without the appropriate scale transformation [Running *et al.*, 1999; Scurlock and Olson, 2002; Zheng *et al.*, 2003; Ahl *et al.*, 2005]. A consistent NPP data set suitable for global NPP model validation is long overdue [Zheng *et al.*, 2003]. Compared to the more studied model validation of climate simulations using observation data, the simulated NPP needs more validations because of the relatively insufficient global data. Thus much work needs to be carried out at the regional and global scale for model validation of NPP.

¹START Regional Center for Temperate East Asia and Key Laboratory of Regional Climate-Environment for Temperate East Asia, Institute of Atmospheric Physics, Chinese Academy of Sciences, Beijing, China.

²National Climate Center, China Meteorological Administration, Beijing, China.

[3] Many studies have been implemented on the NPP simulations with the spatial scale ranging from some sites and local plots, to the entire country and continent for some ecosystem types, and even to global distribution like *Field et al.* [1998] and *Cao et al.* [2005]. The studied temporal scale of terrestrial carbon cycles can be arranged in order as weekly, seasonal, monthly, annual, decadal to geological time [Zeng, 2003] (geological time including such examples as the Holocene [Wang et al., 2005] and the last glacial maximum [He et al., 2005]). Projected simulations under several emission scenarios have been made, e.g., the work of *Cox et al.* [2000], to explore the long-term carbon absorbed by global terrestrial ecosystems from the year of 1850 to 2100. The NPP model intercomparison work [Cramer et al., 1999] can compare the simulated model results and reveal the spatial change of the global terrestrial carbon cycle, however, the same problem of the less model validation still exists because of the inadequate gridded NPP field data.

[4] In recent years, NPP, which is representative of the terrestrial carbon cycle has been incorporated into general circulation models (GCMs), and the terrestrial carbon cycle has been linked to climate change. The physical and biological processes at the land surface coupled to GCMs has been called two-way coupling [Dan et al., 2005]. The two-way coupled model AVIM-GOALS integrates the variation of the terrestrial carbon cycle and climatic change such that the interactive biosphere and atmosphere is revealed, compared to the prescribed structure of terrestrial vegetation like leaf area index (LAI) of some land surface models [Dan et al., 2005].

[5] The objectives of this paper are to (1) use modeled and estimated NPP data sets including the IGBP Global NPP Intercomparison Data and GPPDI Gridded NPP Data to intercompare and validate the NPP simulations at regional (the range of a country, such as China, USA and Australia) and global scales, respectively; (2) reveal the strength and weakness of the IGBP and GPPDI NPP data in the spatial distribution; and (3) explore the relationship between NPP and climate variation in the climate-vegetation coupled model.

2. Model and Data Descriptions

2.1. Atmosphere-Vegetation Interaction Model (AVIM)

[6] AVIM [Ji, 1995] is the land surface model incorporating the physical [Ji and Hu, 1989] and ecophysiological processes. The energy, momentum, and water exchange between land and air is linked with vegetation growth processes and terrestrial ecosystem carbon cycles, which enables the interaction between terrestrial ecosystems and climate. The model has one canopy layer and ten uneven soil layers, and the physical and chemical boundary conditions in the deepest soil layer are assumed constants. The surface hydrological processes include the interception of precipitation and drainage, evapotranspiration from the canopy and evaporation from the ground, surface runoff and infiltration, snowpackage and melting, and water transfer into atmosphere. The canopy photosynthesis, plant respiration and the soil carbon loss through respiration are related to the temperature of the canopy and soil. The vegetation morphology is affected by the accumulation

and consumption of dry matter, and the surface dynamical parameters (such as albedo, zero plane displacement and roughness) as well as resistance parameters, including the stomatal resistance, are affected by the physiological processes.

[7] The NPP equation can be expressed as follows:

$$NPP = GPP - R_m - R_g \quad (1)$$

where GPP is the gross photosynthesis rate excluding photorespiration, R_m is the maintenance respiration rate and R_g is growth respiration rate. GPP is a function of: CO_2 concentration in the stomata, foliage temperature, leaf water potential, the photosynthetic active radiation at the top of canopy and the leaf area index. R_m is function of biomass and vegetation tissue temperature. Ji [1995] has described the details of all the functions.

[8] AVIM has simulated the spatial pattern of NPP and its temporal variation at a seasonal/interannual scale in many basic ecosystems including forests, grasslands, shrublands and croplands [Ji and Yu, 1999; Li and Ji, 2001; Lu and Ji, 2002, 2006]. The simulations reveal the satisfactory variation values of NPP related to changes of air temperature and precipitation. AVIM has participated in the Ecosystem Model-Data Intercomparison (EMDI) organized by IGBP project on Global Analysis, Interpretation and Modeling (GAIM), and the simulated NPP of AVIM agrees well with the measured NPP. The intercomparison result can be found in the figure "EMDI Initial Results: 11 models and field NPP data at 87 sites" and AVIM is the leftmost model, which is detailed at the following website: http://gaim.unh.edu/Structure/Intercomparison/EMDI/phaseIIinfo/ESA_EMDI_p2.ppt.

2.2. Global Ocean-Atmosphere-Land System (GOALS) and the Coupling Strategy

[9] The IAP/LASG GCM GOALS has 9 layers in the atmosphere and is truncated rhombically at the 15 wave numbers [Wu et al., 1996, 1997]. The reduction of a standard atmosphere proposed by Zeng [1963] and Phillips [1973] was used in the dynamical framework to improve the GCM performance. A new k-distribution radiation scheme [Wang et al., 2000] was introduced to make the cloud radiation processes more reasonable. The horizontal resolution is 7.5° longitude by 4.5° latitude. The 1979–1988 monthly mean climatologically observed SST and sea ice were taken from the Atmospheric Model Intercomparison Project (AMIP). The integration time step is 30 min and the land-air coupling is synchronous.

[10] The GOALS GCM developed at the Institute of Atmospheric Physics/State Key Laboratory of Numerical Modeling for Atmospheric Sciences and Geophysical Fluid Dynamics (IAP/LASG), performances well in global climate simulations, especially for the large-scale features and seasonal cycles [Liu et al., 2001]. It has been used to study such climate changes as the maintenance mechanism of the subtropical anticyclone [Liu et al., 2004]. This model was cited in the third IPCC report [Houghton et al., 2001] and used by other scientists to make the future climate projection [e.g., Coquard et al., 2004].

[11] For the purpose of terrestrial ecosystem simulations, the resolution of GOALS is coarse. The land surface model

Table 1. Global Vegetation Classifications [Dan et al., 2005]

Index	Types
1	tropical rainforest
2	broad leaf deciduous trees
3	broad leaf and needle leaf trees
4	needle leaf evergreen trees
5	needle leaf deciduous trees
6	broadleaf trees with ground cover
7	ground cover only
8	broadleaf shrub with ground cover
9	broadleaf shrubs with bare soil
10	dwarf trees with ground cover
11	bare soil
12	crops
13	ice
0	water

AVIM is designed at relatively fine grid of 1.5° by 1.5° , and the interface coupling adopts the nesting technique to link the two models. In other words, a unit grid of the GCM is subdivided into 15 grid cells down to the surface. The two-way coupled model AVIM-GOALS has run for 30 years, and we selected the last 15 years outputs for analysis.

[12] The initial values at land surface were derived from climatological averages of the offline run. The global terrestrial ecosystems were classified into 13 types listed in Table 1 [Dan et al., 2005], and the land cover data was derived from Dorman and Sellers [1989] with modifications for China according to the China Vegetation Map. The global soil texture data were taken from Zabler [1986] with 6 types of classification.

2.3. Climate Data, IGBP NPP Intercomparison Data, GPPDI Gridded NPP Data, and Other Modeled and Estimated NPP Data

[13] In this paper, the global terrestrial surface air temperature and precipitation data were provided by the International Satellite Land Surface Climatology Project Initiative II (ISLSCP II), and the data originated from the Climatic Research Unit (CRU), University of East Anglia. The data set is called CRU05 Mean Monthly Climatology (1961–1990) and its annual average is abbreviated to CRU temperature and CRU precipitation in this study (or CRU data). The data are 0.5° by 0.5° for global land areas excluding Antarctica and have been detailed by New et al. [1999].

[14] The International Geosphere Biosphere Programme (IGBP) Global NPP Model Intercomparison Data (abbreviated to IGBP data here) were used to intercompare the simulated NPP of the two-way coupled model AVIM-GOALS. Global Primary Production Data Initiative (GPPDI) Gridded NPP Data (abbreviated to GPPDI data) were adopted to validate the NPP simulations of the global two-way coupled model. All of the annual mean IGBP and GPPDI NPP data were taken from the Website of ISLSCP II with the resolution of 0.5° by 0.5° . Global terrestrial half-degree IGBP data were derived from the original data containing gridded average NPP for 17 global models of biogeochemistry [Cramer et al., 1999]. GPPDI data [Olson et al., 2001; Zheng et al., 2003] contain 2335 half degree cells, and the field NPP data used to develop 0.5° grid cell estimates come from 15 sources worldwide.

[15] To compare and evaluate the simulated NPP spatial pattern, other NPP data from two global biogeochemical models (CASA and GloPEM), remote sensing data (MODIS NPP) and estimated NPP (ORNL NPP) were adopted in this study. CASA and GloPEM are two representative satellite-based models participating in IGBP NPP Model Intercomparison, and they are driven by NOAA/AVHRR data. The uniqueness is the entire model uses of satellite data of GloPEM without using any climatic driven variables observed on the ground [Cramer et al., 1999]. The multiyear averaged global NPP of CASA model at half degree resolution [Potter, 1999; Potter et al., 2003] can be downloaded at the Website ftp://geo.arc.nasa.gov/pub/glemis/glemis_05/. The global NPP of the GloPEM model at 8 km spatial resolution [Prince and Small, 2003] can be found at the Website <http://glcf.umiacs.umd.edu/data/glopem/>. The multiyear mean GloPEM NPP has been aggregated to global 0.5° grid cell in this study. Improved global 1 km MODIS NPP data averaged during 2000–2003 [Zhao et al., 2006] can be downloaded at <ftp://ftp.ntsg.umd.edu/autofs/MODIS/5/MOD17A3.105.LATEST/>. The data were aggregated to global half degree by Dr. Zhao for our study. The estimated ORNL NPP data for global 2335 0.5° -grid cells [Zheng et al., 2004] were taken from Oak Ridge National Laboratory Distributed Active Archive Center (ORNL-DAAC), which is an update version of the GPPDI data and cover more areas of the three countries in this study.

3. Results and Analysis

3.1. Spatial Distribution of Global and Regional NPP at the Country Level

[16] Prior to presenting the global and the country-level NPP distribution, we make a short validation between the CRU data and the relevant simulations of the global climate. Figure 1 shows the temperature and precipitation of CRU data and the two-way coupled model, and the difference between simulated climate interpolated to a half degree using the bilinear interpolation method and CRU data is also presented. The globally annual mean temperature of AVIM-GOALS (Figure 1a) agrees with CRU temperature (Figure 1b), however, some marked regional biases exist across the globe, such as the cold bias of up to 8°C at northern high latitudes, especially in Eurasia and Greenland (Figure 1c). The lower surface air temperature can be attributed to the insufficient incident radiation in the region with underestimated downward shortwave radiation [Zhang et al., 2002]. A strong warm bias up to 8°C (Figure 1e) occurs along Tibetan Plateau because of the lower surface albedo of thin snow coverage. The simulated annual mean precipitation (Figure 1c) is generally consistent with CRU data (Figure 1d) in the global spatial distribution, but some regional biases are present (Figure 1f). The simulation in the tropical rain forests of Africa, Southeast Asia and South America is higher than CRU precipitation and magnitudes possibly exceeding 4 mm/day. The 2 mm/day overestimated precipitation occurs in eastern China and Australia, and a slightly lower simulation in eastern USA. The area-averaged temperature and precipitation at global and regional scale excluding Antarctica (Tables 2 and 3) shows the overall agreement with CRU data in magnitude despite

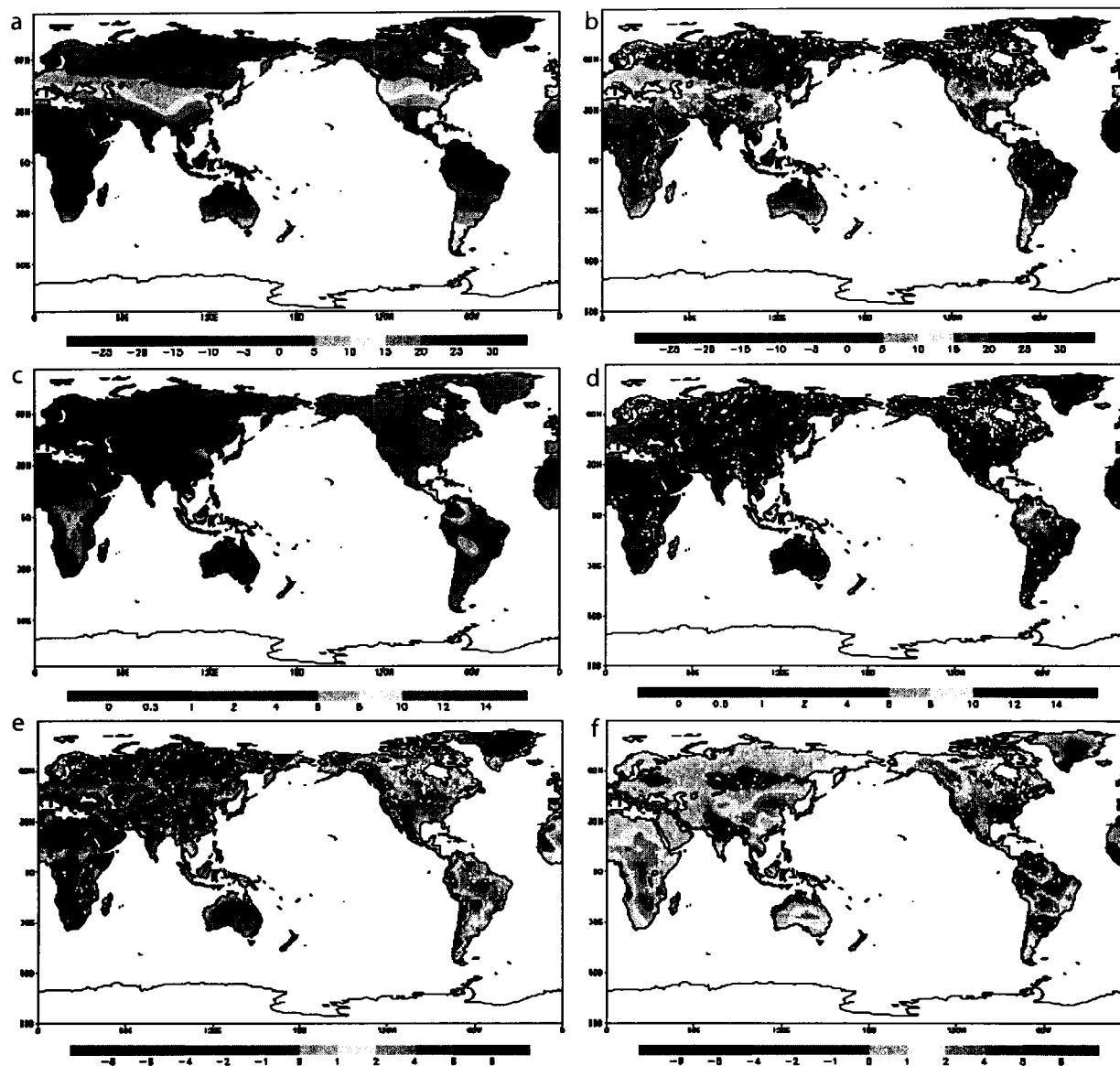


Figure 1. (a) Annual mean surface air temperature of the coupled model; (b) annual mean CRU air temperature from ISLSCP II, with units of °C; (c) annual mean precipitation of the coupled model; (d) annual mean CRU precipitation from ISLSCP II, with units of mm/day; (e) annual mean simulated temperature minus CRU temperature; and (f) annual mean simulated precipitation minus CRU precipitation. (Correlation coefficients of global climatological state are 0.96 for simulated and observed temperature and 0.73 for precipitation, at 99.9% confidence level of t-test.)

the discrepancy of generally higher simulated temperature and precipitation. The global and regional differences between simulated climate and CRU data are comparable to other GCM simulations in the magnitude of the discrepancy with observations, such as the global climate simulation of *Foley et al.* [1998]. The spatial correlation coefficient between simulation and observation is another method to evaluate the performance of the GCM or RCM [Zhou and Qian, 1995; Lau and Nath, 2004] because it can represent the degree of agreement between two spatial patterns of temperature or precipitation [Haywood et al., 1997]. The global spatial correlation coefficient is 0.96 for

temperature and 0.73 for precipitation, which accounts for the fact that precipitation is inherently much noisier spatially than temperature. The values are similar to the coefficients of temperature and precipitation in previous studies, e.g., 0.92/0.5 for GCM and 0.94/0.7 for RCM of *Ju and Wang* [2006].

[17] NPP means the amount of net fixed carbon by vegetation per unit area and per unit time. The vegetation utilizes the photosynthetic active radiation from sunlight to convert the CO₂ into dry matter, which contains the matter and energy for the basic needs of humans. It is a major determinant of carbon sink on land and in the ocean, and a

Table 2. Area-Averaged Surface Air Temperature^a

Time	Area			
	Global T Sim/Obs	China T Sim/Obs	USA T Sim/Obs	Australia T Sim/Obs
DJF mean	6.38/5.70	-1.71/-4.17	-1.09/0.30	32.72/27.58
JJA mean	20.89/19.52	21.41/19.62	25.79/21.96	17.44/15.07
Annual mean	14.29/12.96	11.34/8.55	12.97/11.36	26.11/21.76

^aUnits are °C. T, temperature; Sim, simulation; Obs, CRU observation data; DJF, December-January-February; JJA, June-July-August.

key regulator of ecological processes [Field *et al.*, 1998]. Consequently, many studies [Tian *et al.*, 1999; Cox *et al.*, 2000; Nemani *et al.*, 2003; Lu and Ji, 2006] have been done to determine a quantitative estimate of global and regional NPP, especially under the background of global warming.

[18] Global terrestrial NPP of AVIM-GOALS, IGBP data and MODIS data are shown in Figures 2a–2c. The model intercomparison NPP data (IGBP data) averaged for all 17 models is considered to a comprehensive representation of NPP fluxes [Cramer *et al.*, 1999]. MODIS NPP is the first continuous satellite-driven data set for repeated monitoring of global vegetation productivity at 1-km resolution over vegetated land at an 8-day interval [Zhao *et al.*, 2005, 2006]. The simulated NPP is similar to the IGBP data and MODIS NPP, with the highest NPP (>1000 g C m⁻² year⁻¹) in the tropical rain forests, the intermediate NPP (500–700 g C m⁻² year⁻¹) in temperate regions, and the lowest NPP (<200 g C m⁻² year⁻¹) in the cold or arid regions. However, the simulated NPP in boreal forests and tundra exhibits an obviously lower NPP belt (same hereafter), which is mainly due to the cold bias (Figure 1a) limiting the vegetation growth especially in boreal summer. For instance in northwest Europe (10–20°E), the simulated NPP can be 200 g C m⁻² year⁻¹ lower than IGBP data south of 63°N. When validating the simulated NPP further in Sweden using GPPDI data (figure not shown here), we found that the simulated NPP in southern Sweden (56–63°N and centered 15°E) appears to be around 120 g C m⁻² year⁻¹ lower because of the cold bias, and IGBP data are at least 150 g C m⁻² year⁻¹ overestimated, given that the GPPDI NPP from field data is regarded as an actual distribution. In the Southern Hemisphere, the simulated NPP south of 15°S in Africa is larger than IGBP data mainly because of the vegetation type classification of broadleaf trees in contrast with the shrublands or grassland in other models such as C3 and C4 grasslands of BIOME-BGC [Running and Hunt, 1993; Hunt *et al.*, 1996]. The broadleaf trees under overestimated temperature and precipitation can lead to the higher NPP simulation.

[19] For the sake of deep validation of NPP in spatial pattern, we present the simulated NPP of China, USA and Australia because GPPDI data do indeed have measured values in these three countries (available data is sparse over

China). Figure 3 shows the simulated NPP (Figure 3a), IGBP data (Figure 3d) and MODIS NPP (Figure 3e) in China. To compare the simulated NPP to other models, regional NPP of CASA and GloPEM is also presented in Figures 3b and 3c. The simulated NPP in eastern China south of 35°N is consistent with IGBP and MODIS data in that the magnitude is larger than 500 g C m⁻² year⁻¹ and reaches 700 g C m⁻² year⁻¹ more in southern China, which reflects the relatively large carbon flux in this area corresponding to the largest water and heat conditions for vegetation growth over China. The CASA and GloPEM model shows the similar spatial pattern with the exception of generally higher value of GloPEM and lower of CASA in southern China. The spatial pattern is reasonable compared to the modeled result of Tao *et al.* [2003] using the NOAA NDVI in the CEVSA model [Cao and Woodward, 1998] to calculate the climatological NPP distribution of China. Tao *et al.* [2003] shows a similar pattern south of 35°N in China, and other studies [e.g., Sun and Zhu, 2001; Chen *et al.*, 2002] use remote sensing data of vegetation to estimate the terrestrial NPP of China, presenting the same NPP magnitude south of 35°N in China. However, the NPP in northeast China simulated by AVIM-GOALS is much lower than IGBP and MODIS data, especially north of 48°N, which can be attributed to underestimated air temperature reaching 4°C. However, it is interesting to explore the actual NPP in this area further. Jiang *et al.* [1999] used the ground-based measurements of NPP from Forestry Ministry of China [1994] to present the spatial distribution of NPP in China. Their subdivided areas (9A, 9B and 10B) sum equivalent to the area north of 48°N in this study shows the NPP ranging from 301.5 to 342 g C m⁻² year⁻¹. The GPPDI data in this area is mainly 350–400 g C m⁻² year⁻¹. The simulated NPP of Tao *et al.* [2003] and the calculation of Wang *et al.* [2001] using the model of Zhou and Zhang [1995] show also the similar ranges. Consequently, we consider that the value 350–400 g C m⁻² year⁻¹ seems to be the actual NPP north of 48°N in northeast China, which is reflected in MODIS data. The new calculated NPP of Cao *et al.* [2005] using AVHRR land data and observational climate to drive the GloPEM model over China (Figure 3f) and the NPP of ORNL data (Figure 3g), present the same NPP magnitude in this area. For the NPP distribution in western China, the

Table 3. Area-Averaged Precipitation^a

Time	Area			
	Global P Sim/Obs	China P Sim/Obs	USA P Sim/Obs	Australia P Sim/Obs
DJF mean	2.64/2.01	1.68/0.44	1.93/1.71	2.86/2.41
JJA mean	2.51/2.45	3.37/4.33	1.97/2.30	1.02/0.68
Annual mean	2.70/2.15	2.57/2.00	1.95/1.98	1.89/1.31

^aUnits are mm/day. P, precipitation; Sim, simulation; Obs, CRU observation data; DJF, December-January-February; JJA, June-July-August.

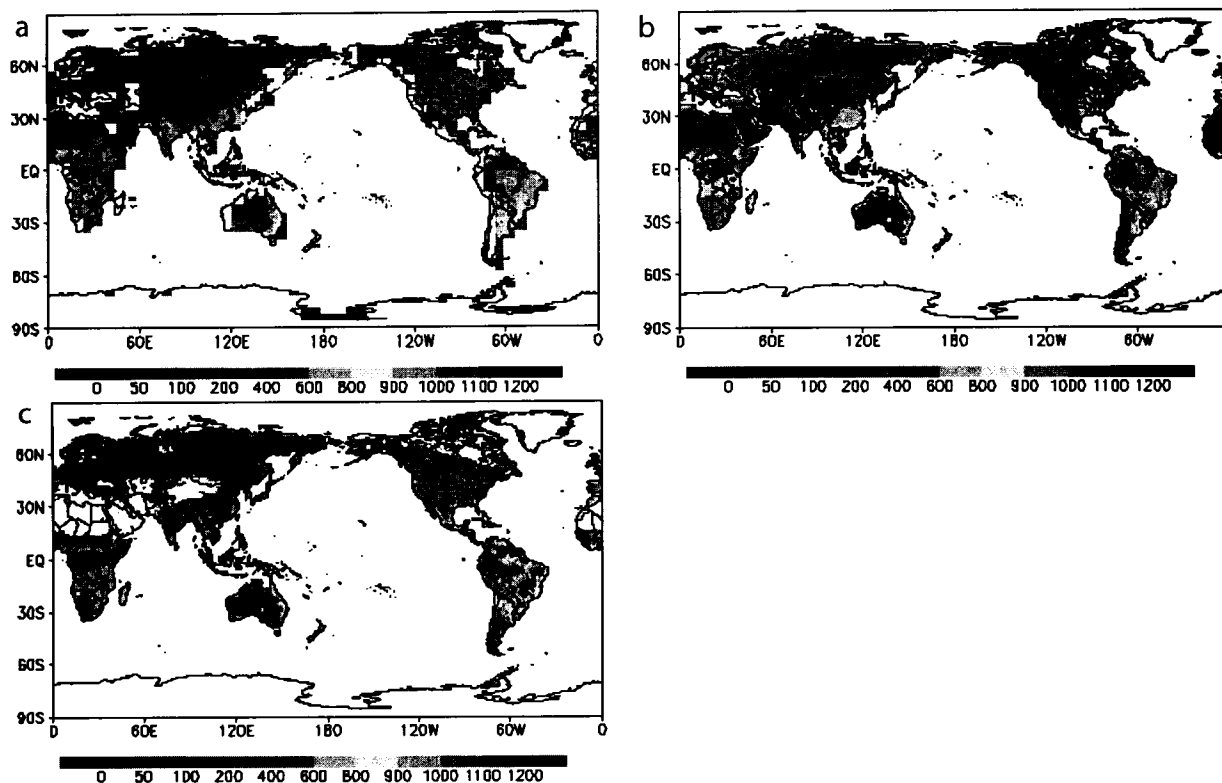


Figure 2. Globally annual mean NPP of (a) the coupled model AVIM-GOALS, (b) IGBP Global NPP Intercomparison data from ISLSCP II, and (c) MODIS NPP data. Units are $\text{g C m}^{-2} \text{ year}^{-1}$.

simulated NPP west of 95°E agrees well with IGBP data and the agreement is consistent with the work of *Tao et al.* [2003].

[20] Figures 4a–4g present the simulated annual mean NPP, modeled NPP (CASA and GloPEM), IGBP data, MODIS data, GPPDI data and ORNL data of USA respectively. Compared to the estimated and modeled NPP data (CASA and GloPEM), the simulated NPP reproduces the high NPP in the southeastern USA and low values in the northwest. However, the simulated NPP in the central USA south of 40°N is overestimated because of the high temperature and precipitation. The maximum discrepancy is located in northeast USA north of 36°N , where the simulation is much lower than the IGBP data, GPPDI data and ORNL data. The reason for the markedly lower magnitude up to $400 \text{ g C m}^{-2} \text{ year}^{-1}$ in the northeastern corner of USA is complicated, since the annual temperature and precipitation of the two-way coupled models agrees generally with the CRU data. We assumed that one of the potential causes is the radiation (not analyzed in this study) affecting the photosynthetic active radiation (PAR) at the top of the canopy, because the solar radiation in the eastern USA is one potential climatic constraint to plant growth according to *Nemani et al.* [2003]. It is interesting that the MODIS data in northeastern corner (Figure 4e) are also lower than GPPDI and ORNL data, which demonstrates the complicated NPP distribution for different data sets and the necessity of validating NPP at a regional scale.

[21] The simulated and other NPP data over Australia (not including Tasmania) are shown in Figure 5. All of the

NPP values show the decreasing trend from east, north and southwest to central Australia. NPP of the coupled model shows intermediate values, with magnitudes ranging between CASA and GloPEM in most regions. The simulated NPP in eastern part can reach $800\text{--}1100 \text{ g C m}^{-2} \text{ year}^{-1}$ similar to the IGBP and MODIS data, which reflects the sufficient heat and water conditions for vegetation growth, but the simulation band is much wider than the IGBP and MODIS data with the highest NPP located along the eastern coasts. According to the document of ISLSCP II for the GPPDI data, there are possible lower estimates of belowground NPP (consequently for total NPP as well) for shrubland cells in Australian data because of application of belowground/aboveground carbon allocation method [*Raich and Nadelhoffer*, 1989] that is more suitable for forest ecosystems. We can see that the GPPDI data in central Australia are almost below $100 \text{ g C m}^{-2} \text{ year}^{-1}$ (Figure 5f); the simulation, IGBP and MODIS data can range from 200 to $300 \text{ g C m}^{-2} \text{ year}^{-1}$, and this discrepancy maybe reflects the possible underestimate of the GPPDI NPP in this area.

[22] To compare the NPP magnitude at global and national levels, area-averaged NPP for all models and estimated data is presented in Table 4. Compared to the global and regional averaged NPP of IGBP and MODIS data, the simulation shows the agreement in global NPP, lower NPP magnitudes in China and USA, and higher magnitudes in Australia. The reason is the underestimated NPP of boreal forests in northeast China and northeast USA, and the wider distribution of high NPP in eastern Australia affected

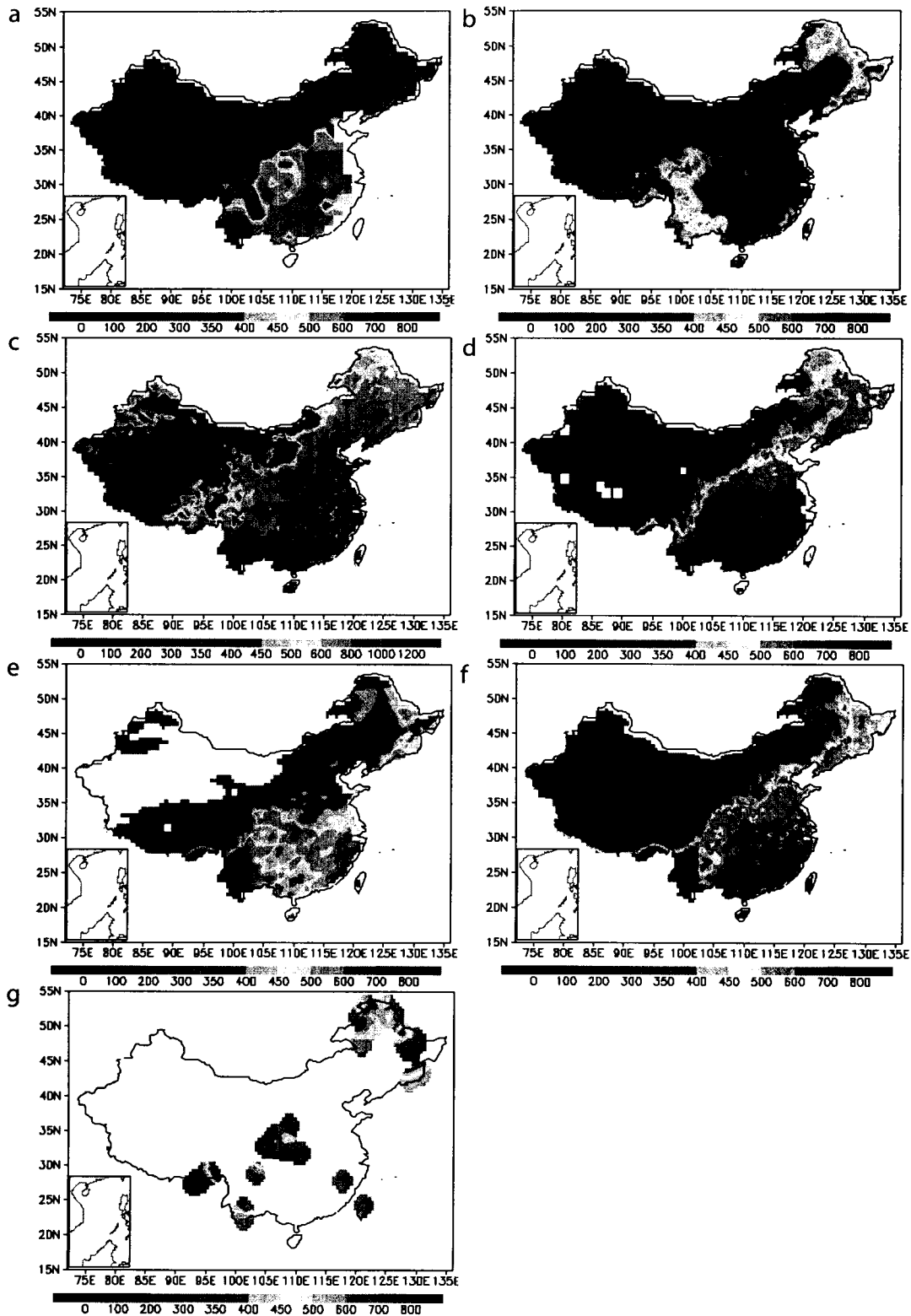


Figure 3. Annual mean NPP over China of (a) AVIM-GOALS, (b) CASA, (c) GloPEM, (d) IGBP Global NPP data from ISLSCP II, (e) MODIS NPP data, (f) GloPEM from *Cao et al.* [2005], and (g) ORNL estimated data. Units are $\text{g C m}^{-2} \text{ year}^{-1}$.

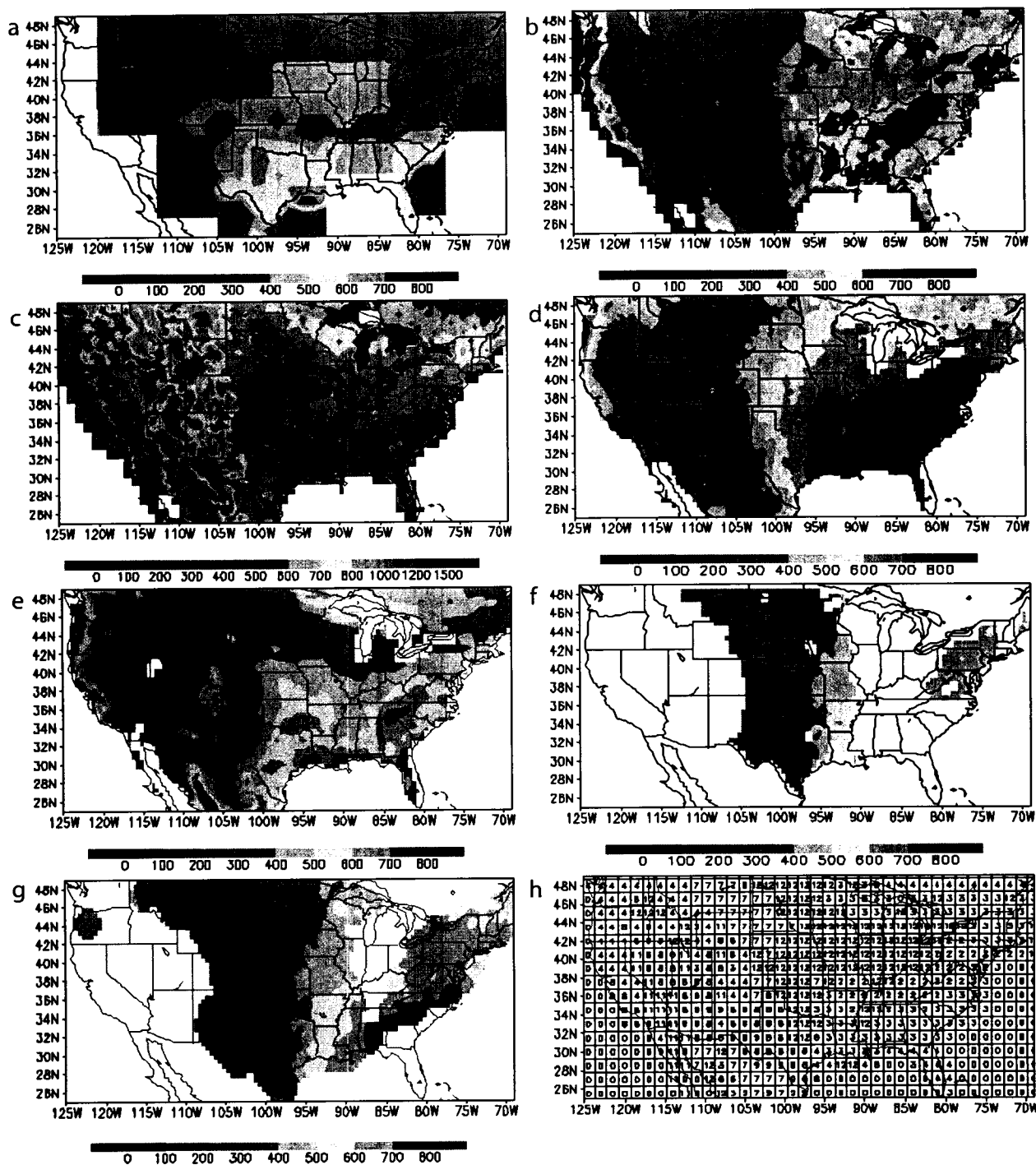


Figure 4. Annual mean NPP over USA of (a) AVIM-GOALS, (b) CASA, (c) GLoPEM, (d) IGBP Global NPP data from ISLSCP II, (e) MODIS data, (f) GPPDI Gridded data from ISLSCP II, and (g) ORNL estimate data. Units are $\text{g C m}^{-2} \text{ year}^{-1}$. (h) Land cover classifications over USA (see Table 1 for the specification).

mainly by overestimated precipitation. The simulated NPP lies between CASA and GLoPEM modeled values at global and regional scale. The values of *Cao et al.* [2005] over China and ORNL data over USA demonstrate the slightly high NPP of China and $90 \text{ g C m}^{-2} \text{ year}^{-1}$ high in USA for

IGBP NPP data, whereas MODIS NPP shows an approximate magnitude in the two countries. Global higher averaged MODIS NPP in comparison to IGBP data results in part from the high NPP of $5^{\circ}\text{S} - 30^{\circ}\text{N}$ due to the lower vapor pressure deficit (VPD) [Zhao et al., 2006]. To study the

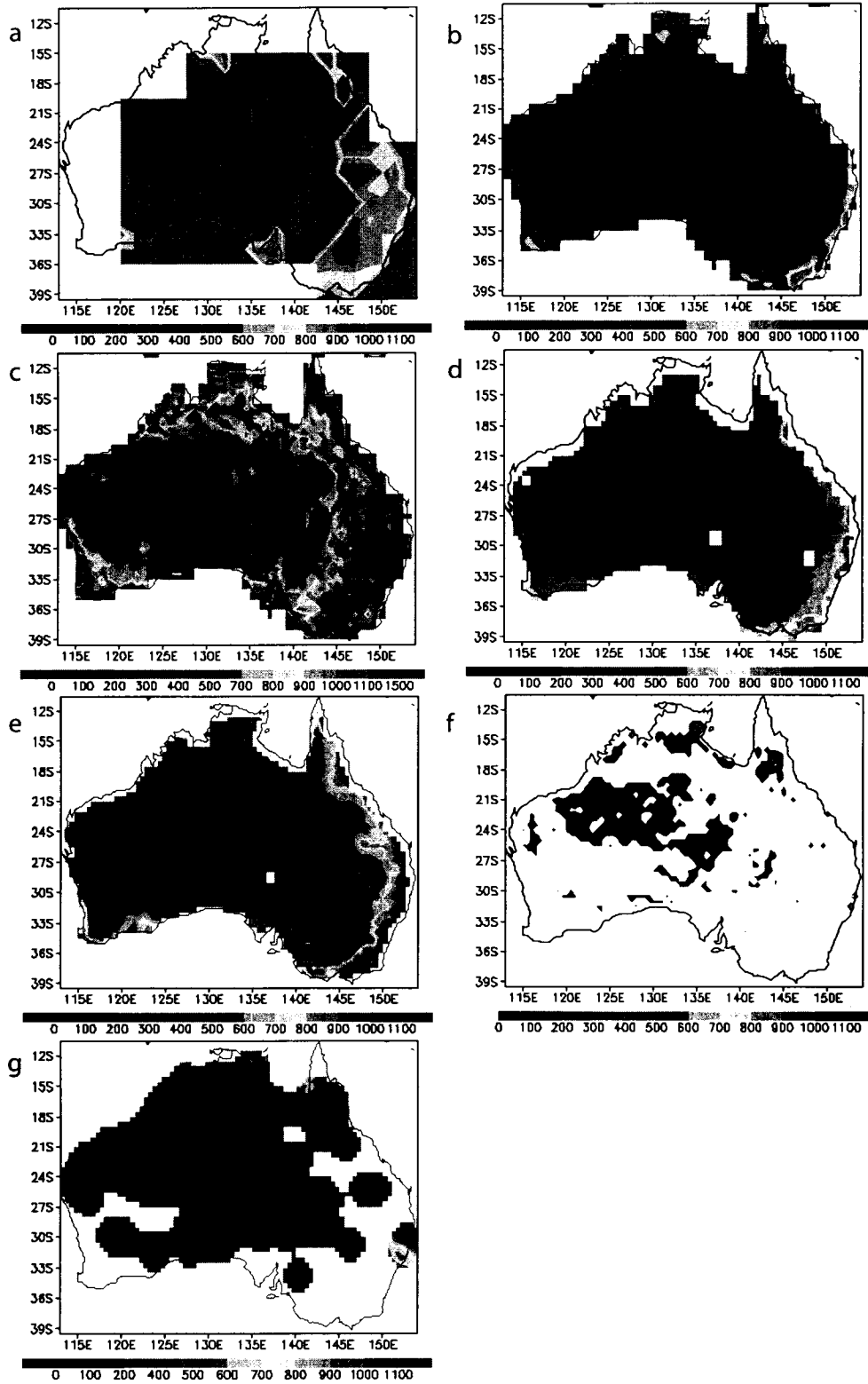


Figure 5. Legend as Figures 4a–4g but for Australia.

Table 4. Area-Averaged Annual NPP at Global and Country-Level Scale^a

NPP Origin	Global Average	Average Over China	Average Over USA	Average Over Australia
AVIM-GOALS	447.47	330.83	309.13	459.33
CASA NPP	313.99	331.79	387.57	251.54
GloPEM NPP	744.84	745.66	814.78	664.49
IGBP NPP data	450.42	417.58	497.73	300.26
MODIS NPP data	505.85	405.50	409.36	354.27
Other NPP		391.14 ^b	402.96 ^b	

^aUnits are $\text{g C m}^{-2} \text{ year}^{-1}$.

^bNPP value of *Cao et al.* [2005] over China using GloPEM model and ORNL data over USA.

spatial agreement between the simulated NPP and other data, MODIS NPP was dealt with the referenced NPP to calculate the correlation coefficients of NPP values. The correlation coefficients have a high statistical significance of 99.9% in a student t-test and are shown in Table 5. For all NPP values, the lowest correlation occurs in the USA. For the three countries, AVIM-GOALS shows the largest correlation in China, whereas CASA and GloPEM have largest values in Australia. The correlation coefficient of AVIM-GOALS is located between CASA and GloPEM for global average. IGBP NPP shows the largest correlation at global and the country-level scale in contrast with other NPP sources. The coefficients reflect the agreement of AVIM-GOALS NPP with MODIS data lies between CASA and GloPEM for global average, and IGBP NPP agrees spatially well with MODIS data.

[23] In this study, a relative error term (RE), as adopted by *Zhao et al.* [2006], was used to evaluate the simulated NPP uncertainty at regional and global scale against IGBP data, and RE equation is:

$$RE = \frac{\sum_{i=1}^n \frac{P_i - P_r}{P_r}}{n} \times 100\% \quad (2)$$

where P_i is global and regional NPP of models, P_r is IGBP data, n is the number of grid cells. Table 6 presents the RE values of AVIM-GOALS, CASA and GloPEM at global and regional scale. A significant discrepancy exists for the three models: AVIM-GOALS has positive RE values of globe and Australia and negative in China and USA, whereas CASA is negative and GloPEM is positive at regional and global scales. The simulated RE values are largest in Australia (>60%) and relatively small in other regions. The global RE value is a quantitative measure of the deviation between AVIM-GOALS and IGBP NPP. This is comparable to CASA and GloPEM and the degree of departure from global IGBP NPP in the coupled model is located between the two models.

3.2. Zonal Average and Latitudinal-Seasonal Variation of Global NPP

[24] Figure 6 is the globally zonal average for surface air temperature, precipitation and NPP distribution. All zonal

mean NPP values (Figure 6c) show the similar latitudinal variation pattern despite the different magnitude. The simulated NPP is close to IGBP and MODIS data except for north of 45°N, and the magnitude varies between CASA and GloPEM in 45°N–50°S. The zonal mean temperature over land south of 50°N is above 0°C, which is reflected in the simulation and CRU temperature. The climatic factors of temperature, precipitation and radiation (not analyzed here) tend to be colimiting the plant growth [*Nemani et al.*, 2003]. This study only considers precipitation and temperature at regional and global scales, which are the two major climatic factors that govern the NPP of the biosphere [*Cramer et al.*, 1999; *Tian et al.*, 1999]. In boreal regions, the vegetation is mainly controlled by air temperature; in temperate regions, the vegetation growth is affected by temperature and precipitation; in subtropical and tropical regions, the precipitation is the principal limiting factor for the vegetation growth because of the sufficient surface heat content. Consequently, the NPP discrepancy in Figure 6c is related to the climate difference (Figures 6a and 6b). The simulated zonal mean NPP north of 50°N is lower than the IGBP and MODIS data, which reflects the lower temperature in this region. For the NPP distribution in the Arctic Circle, the ecosystem is mainly tundra and the absolute value of NPP is rather low, thus the magnitude of the NPP discrepancy is not large despite the lower temperature up to 10°C. However, the question remains as to why the 30–50°N zonal mean NPP is obviously smaller than the IGBP and MODIS data since the simulated temperature is 1–2° higher than the CRU data and the simulated precipitation is slightly overestimated. Through careful analysis, we found the cause originating over the Tibetan Plateau, where the simulated strong warming bias more than 8°C (Figure 1e) leads to the slight overestimate of zonal mean temperature between 30 and 50°N, with the explanation being the thin snow cover [*Dan et al.*, 2005]. However, the obvious warming in the Tibetan Plateau cannot cause the corresponding NPP increase in full, because the land cover is bare soil or sparse vegetation in arid regions. So the underestimated temperature in other regions along this latitude results in the well-defined decrease in NPP (e.g., northeast China for conifer forests, see Figure 3a). For the

Table 5. Correlation Coefficients Between NPP Values and MODIS NPP Data in the Global and Country-Level Spatial Pattern

NPP Origin	Globe	China	USA	Australia
AVIM-GOALS	0.77	0.76	0.57	0.63
CASA NPP	0.82	0.64	0.64	0.80
GloPEM NPP	0.72	0.65	0.45	0.70
IGBP NPP data	0.86	0.81	0.75	0.90

Table 6. Relative Error Term (RE) of the Three Global Models With Respect to IGBP NPP Data

Global/Regional RE	AVIM-GOALS, %	CASA, %	GloPEM, %
Globe	20.01	–16.47	106.27
China	–20.71	–18.37	96.09
USA	–31.96	–16.78	107.32
Australia	64.41	–10.58	161.36

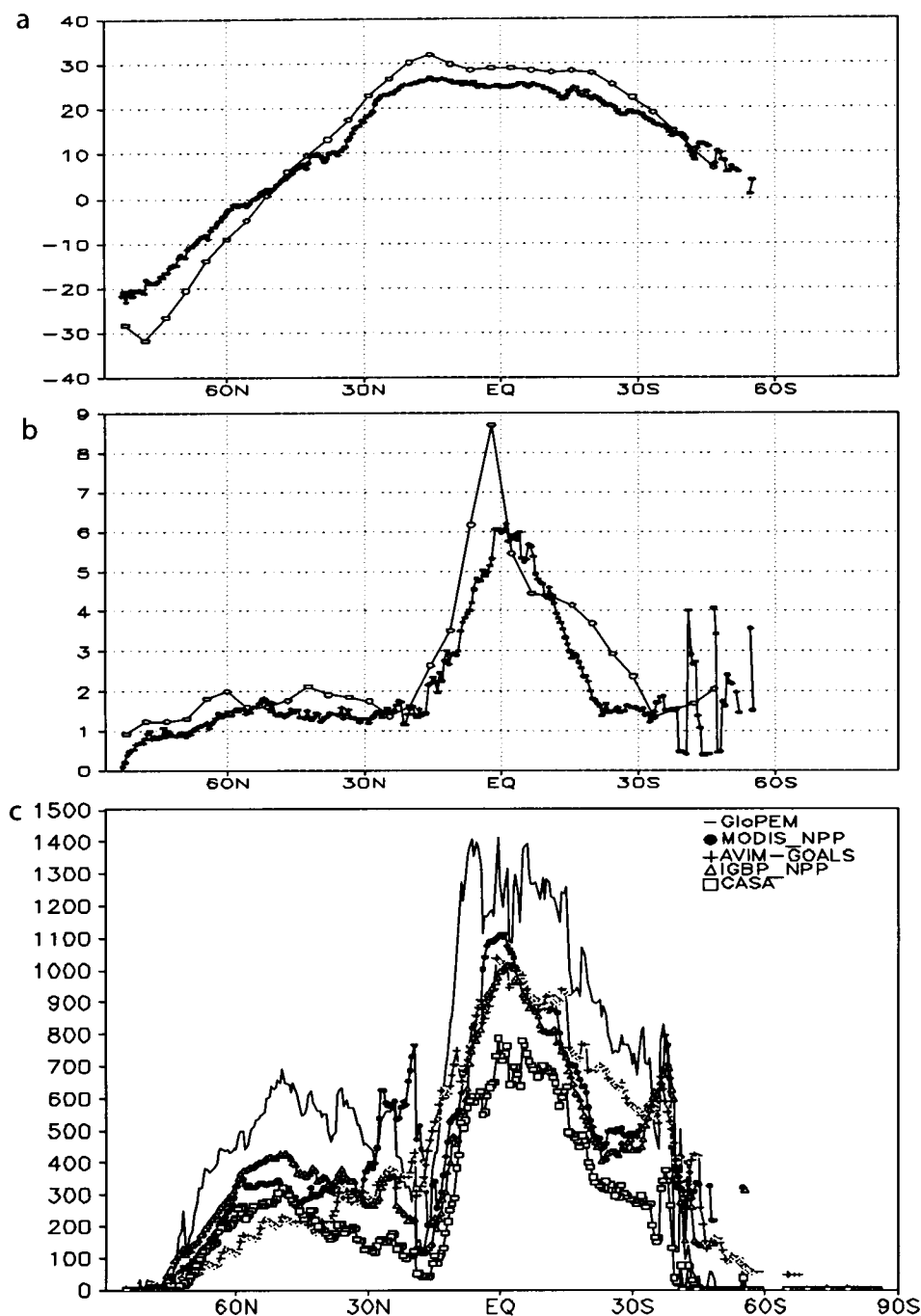


Figure 6. Zonal average of the annual means: (a) surface air temperature, with units of °C; (b) precipitation, with units of mm/day, open circle indicates outputs of AVIM-GOALS, and solid circle indicates CRU climate; and (c) NPP of three global models, IGBP NPP data and MODIS data, with units of $g\ C\ m^{-2}\ year^{-1}$.

zonal mean NPP between 30°N–30°S, the NPP variation is mainly controlled by precipitation change, and the overestimated NPP simulation (in contrast with IGBP and MODIS data) generally corresponds to the increasing precipitation magnitude compared to CRU data (Figure 6b).

The 5°S–30°N MODIS NPP is overestimated because of the lower vapor pressure deficit [Zhao *et al.*, 2006], thus it presents NPP values which are too high between 20 and 30°N. By comparing the overall trend of zonal mean curves of NPP with that of air temperature and precipitation, we

Table 7. Zonal Mean of Annual NPP for Latitudinal Bands With 30° Interval^a

NPP Origin	60–30°S Average	30°S–0° Average	0–30°N Average	30–60°N Average	60–90°N Average
AVIM-GOALS	470.76	791.89	493.18	216.83	70.92
CASA NPP	311.71	564.86	318.93	253.68	146.73
GloPEM NPP	848.71	1182.55	846.09	626.59	387.35
IGBP NPP data	453.58	672.40	451.53	380.43	214.78
MODIS NPP data	506.32	737.38	678.61	325.78	180.13

^aUnits are $\text{g C m}^{-2} \text{ year}^{-1}$.

found that the NPP variation across latitudes is more similar to precipitation change than it is to temperature.

[25] The zonal mean NPP in the latitudinal band is generally consistent with IGBP and MODIS data (Table 7), however, the values above 60°N is markedly underestimated for the same reason for China and USA. The largest NPP distribution was found between 30°S–30°N, whereas the NPP of 0–30°N is smaller than that of 30°S–0 because of more arid regions or deserts in the 0–30°N belt. The simulated value is located between CASA and GloPEM excluding the northern high latitude. This suggests again that the simulated NPP magnitude varies generally between the two global biogeochemical models and the latitudinal NPP variation of the coupled model is reasonable in comparison to IGBP and MODIS data. The high NPP of MODIS data in the regions 30°S–0 and 0–30°N has an identical explanation to that of the 5°S–30°N.

[26] Figure 7 exhibits the month-to-month change of climate and simulated NPP across latitudes. The latitudinal-seasonal change of simulated air temperature agrees well with the CRU temperature, with a discrepancy of 5° overestimate between 30°S and 30°N. During June to August in each semihemisphere, a temperature ridge exists representing a cold peak in the Southern Hemisphere and a warm peak in the Northern Hemisphere, especially poleward of 30°S or 30°N. The simulated and CRU precipitation shows the latitudinal-seasonal pattern similar to the temperature and the main rain belt is located in the tropical regions. The simulated monthly NPP with the magnitude above 60 g C m^{-2} is mainly located in the 10°S–5°N tropical belt, which corresponds to the largest air temperature and precipitation in this latitudinal zone. The NPP in northern latitudes above 30°N shows the maximum value during boreal summer related to the climate ridge especially to temperature. The region poleward of 30°S has the lowermost NPP during June to August, but it is not as obvious as the peak of the Northern Hemisphere because of the fact that most landmasses in the Southern Hemisphere are mainly distributed within the relatively warm conditions of 35°S. The NPP in the tropical latitudes exhibits no peaks or conspicuous low values, which can be attributed to the fact that the different seasonal patterns (but of similar magnitudes) of NPP in Northern and Southern Hemisphere oppose each other, acting as buffers. Also, the latitudinal-seasonal variation of globally monthly NPP should be correct when compared with the results of the 15 models participating in the Potsdam NPP model Intercomparison Workshop [Kicklighter *et al.*, 1999].

3.3. Global NPP and Climate for Vegetation Type

[27] It is rather difficult to obtain global field data of NPP to validate global or regional models, but use of the

averaged NPP by biome type is a valuable method to evaluate the terrestrial NPP [Zhao *et al.*, 2005]. The intercomparison of NPP by vegetation types has been used in many previous studies [Scurlock and Olson, 2002; Dan *et al.*, 2005; Zhao *et al.*, 2005] and it proves to be a useful validation method for global NPP distribution. Global NPP averaged by biome types is shown in Figure 8a for 11 vegetation types excluding bare soil or desert, and the vegetation classification can be found in Table 1. Similar to NPP, the simulated and observed climate (temperature and precipitation) for the 11 vegetation types is also presented in Figures 8b and 8c.

[28] NPP of all sources show high values in tropical rain forest (vegetation 1), broadleaf trees with ground cover (vegetation 6) and crops (vegetation 12), which can be attributed to the favorable climate conditions for vegetation growth in the two former types and the human effects (e.g., irrigation) in the latter. The lower NPP occurs in arid or cold regions (vegetation 9 and 10) with unfavorable growth conditions of climate. The simulated NPP of AVIM-GOALS in boreal forest (types 3–5) and tundra (type 10) is lower than IGBP and MODIS NPP because of the underestimated temperature, especially for vegetation type 5, and the simulated NPP of other vegetation types lies generally between CASA and GloPEM. The averaged NPP for all NPP sources (Figure 8a) is highly correlated to mean climate of precipitation (Figure 8c) with a correlation coefficient of 0.96, which is higher in magnitude and statistical significance than those of temperature (0.59). This shows that the NPP variation across global vegetation types depends highly on precipitation and temperature is generally the second climate constraint. The correlation coefficients between the simulated and observed climate (0.98 for temperature and 0.93 for precipitation) reflect the good agreement of actual climate data to simulated climate data across terrestrial ecosystem types excluding bare soil. All the coefficients are conducted in a student t-test and the significance level is shown in the Figure 8 legend.

[29] To evaluate further the uncertainty of NPP for biome types in the variation amplitude, the maximum, minimum and range (Max-Min-Ran) of NPP are presented in Figure 9. The NPP range of AVIM-GOALS is higher than IGBP and MODIS data, and the range of MODIS NPP corresponds closely to that of mean NPP averaged in all NPP sources (Figure 9a). The maximum and minimum simulations are located in the intermediate position for the three global models. The Max-Min-Ran of each NPP source minus that of mean NPP is shown in Figure 9b. The simulated range difference of AVIM-GOALS can be more than $100 \text{ g C m}^{-2} \text{ year}^{-1}$, and the Max-Min difference lies again between CASA and GloPEM. The comparison reflects that the smallest discrepancy with respect to averaged NPP occurs

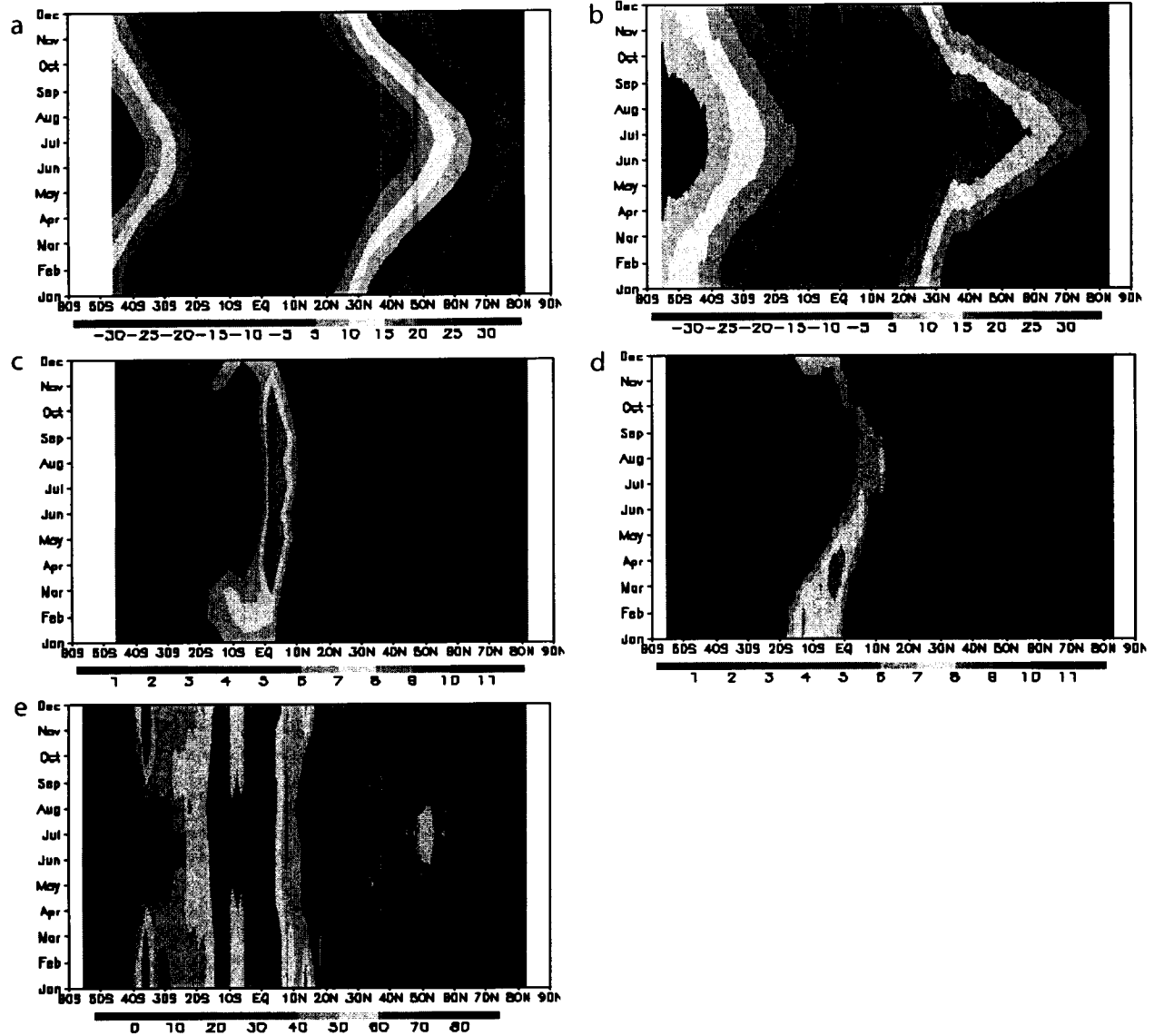


Figure 7. Month-to-month variation for globally zonal mean of annual NPP and climate: (a) surface air temperature (T_s) of AVIM-GOALS; (b) CRU T_s data, with units of $^{\circ}\text{C}$; (c) precipitation of AVIM-GOALS; (d) CRU precipitation data, with units of mm/day ; and (e) NPP of AVIM-GOALS, with units of $\text{g C m}^{-2} \text{ month}^{-1}$.

in MODIS NPP, and IGBP NPP is second to MODIS data. Thus the Max-Min-Ran relative percentage (RP) with respect to MODIS data is calculated as:

$$RP = \frac{P_i - P_m}{P_m} \times 100\% \quad (3)$$

where P_i is the Max-Min-Ran of three global models and IGBP NPP, P_m is the Max-Min-Ran of MODIS NPP data. The RP values of AVIM-GOALS (Figure 9c) lie within $\pm 20\%$ and resemble those of IGBP NPP data, which reflects the relative agreement with IGBP and MODIS data. The absolute RP value of GloPEM range is the smallest in the three global models and agrees well with IGBP and MODIS data. The Max-Min RP value of AVIM-GOALS is located between CASA and GloPEM. The absolute RP values of

IGBP data are lower than 15%, which shows the closest agreement with MODIS data.

[30] Finally, the correlation coefficient (Corr) between NPP and the observation climate is calculated to explore the relationship of global NPP with temperature and precipitation for vegetation types. All the coefficients and their significance level in a student t-test are presented in Table 8. The Corr of all NPP with precipitation is statistical high compared to that of temperature. The Corr of temperature for the simulated NPP is highest in all NPP sources, and the Corr of precipitation is smallest compared to that of other NPP sources. This reflects that the NPP variation of global vegetation types in the coupled model is more related to temperature than other NPP data, which helps to understand the lower simulated NPP at northern high latitudes due to

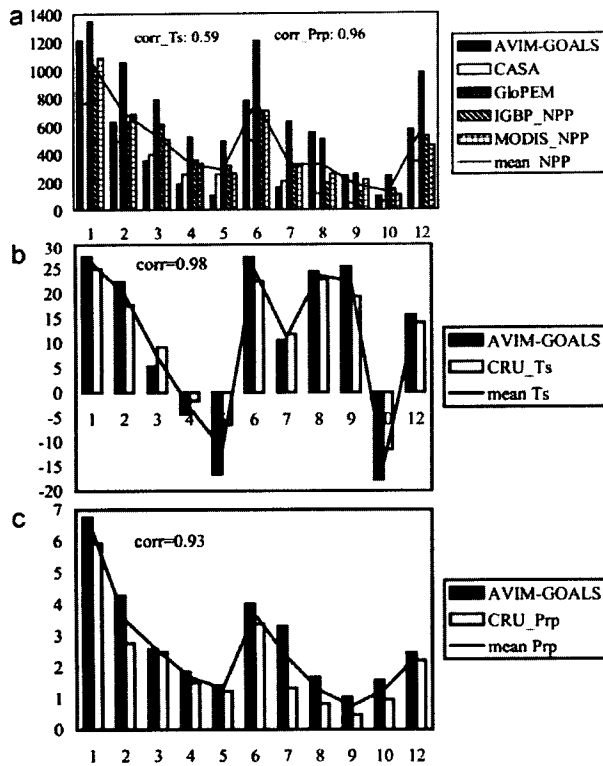


Figure 8. Annual mean NPP and climate based on global vegetation type: (a) NPP, with units of $\text{g C m}^{-2} \text{ year}^{-1}$; (b) surface air temperature, with units of $^{\circ}\text{C}$; and (c) precipitation, with units of mm/day . (corr, correlation coefficient between the simulated climate and CRU data at 99.9% significance level; corr_Ts, correlation coefficient of mean NPP with mean temperature at 90% significance level; corr_Prp, correlation coefficient of mean NPP with mean precipitation at 99.9% significance level.)

the underestimated temperature. The Corr of MODIS data shows the highest correlation with temperature and precipitation and equals nearly to the Corr of mean NPP, which exhibits the high dependence on temperature and precipitation across global biome types. IGBP Corr shows stronger correlation with precipitation than temperature, as opposed to MODIS data.

[31] For all NPP sources, vegetation type 8 (broadleaf shrub with ground cover) is the main type leading to the lower Corr with climate. To show this effect, the Corr removing type 8 is shown in Table 9. The simulated Corr for precipitation increases to 0.95, and the Corr of other NPP data increases markedly for temperature, especially in CASA model. This reflects the different mechanism of vegetation type 8 related to climate: controlled by precipitation and not simulated well in the coupled model; controlled mainly by temperature and possibly not captured well in other two global models, IGBP and MODIS data.

4. Conclusions and Discussion

[32] The global model NPP, ranging from 39.9 to 80.5 Pg C year^{-1} [Cramer et al., 1999], indicates a large uncertainty

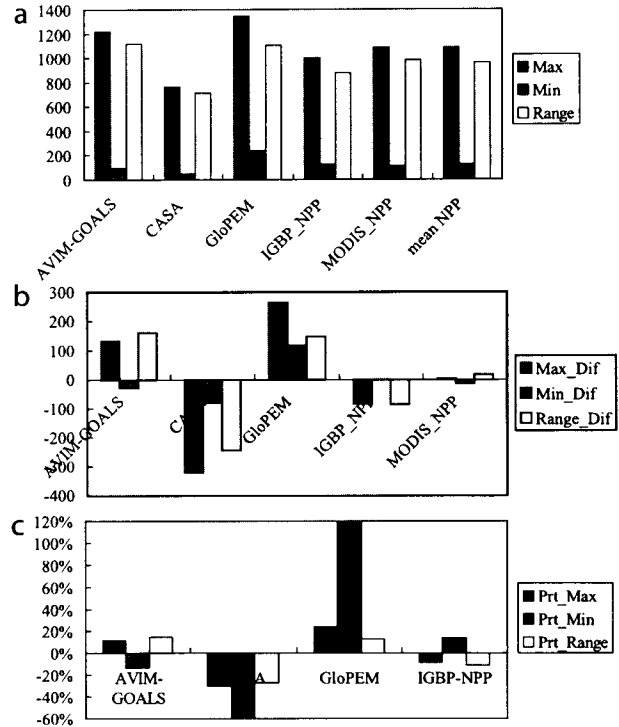


Figure 9. Maximum, minimum and range of NPP by global vegetation type for all data sets: (a) NPP and their average; (b) the difference of NPP minus the mean values in Figure 9a, with units of $\text{g C m}^{-2} \text{ year}^{-1}$; and (c) relative percentage of NPP with respect to MODIS data in the equation of $(P_i - P_m)/P_m$ multiplying by 100%, P_m is NPP from MODIS data. (Max, maximum; Min, Minimum; Dif, difference; Prt, percentage.)

[Ahl et al., 2005]. Consistent data on terrestrial NPP are urgently needed to constrain model estimates of carbon fluxes and hence to refine our understanding of ecosystem responses to climate change [Scurlock and Olson, 2002]. However, because of the long-term deficiency of global data [Zheng et al., 2003; Zhao et al., 2005], the model NPP validation is not implemented fully and maturely at global and regional scales as are the validations of climatic simulations. Many discrepancies exist for global NPP estimates, such as in the tropical rain forests, the maximum of $850 \text{ g C m}^{-2} \text{ year}^{-1}$ for Field et al. [1998], $964 \text{ g C m}^{-2} \text{ year}^{-1}$ for Cao and Woodward [1998], 1500 g C m^{-2}

Table 8. Correlation Coefficients Between All NPP and CRU Climate by Global Vegetation Type^a

NPP Origin	Corr_Ts and the Significance Level	Corr_Prp and the Significance Level
AVIM-GOALS	0.76 (99%)	0.88 (99.9%)
CASA NPP	0.46 (80%)	0.97 (99.9%)
GloPEM NPP	0.60 (99%)	0.90 (99.9%)
IGBP NPP data	0.47 (80%)	0.97 (99.9%)
MODIS NPP data	0.60 (95%)	0.97 (99.9%)
Mean NPP	0.61 (95%)	0.96 (99.9%)

^aTs, air temperature; Prp, precipitation. The significance level in the parentheses is obtained in a student t-test.

Table 9. Correlation Coefficients Between All NPP and Climate as Table 8 but for Excluding Vegetation Type 8 of Broadleaf Shrub With Ground Cover

NPP Origin	Corr_Ts and the Significance Level	Corr_Prp and the Significance Level
AVIM-GOALS	0.77 (99%)	0.95 (99.9%)
CASA NPP	0.61 (90%)	0.96 (99.9%)
GloPEM NPP	0.71 (98%)	0.90 (99.9%)
IGBP NPP data	0.63 (95%)	0.97 (99.9%)
MODIS NPP data	0.73 (98%)	0.97 (99.9%)
Mean NPP	0.71 (99%)	0.97 (99.9%)

year⁻¹ for Goetz *et al.* [2000], 1672 g C m⁻² year⁻¹ for Bonan *et al.* [2003] and 1000 g C m⁻² year⁻¹ for Zeng [2003]. There is a need for improved understanding of the factors that influence the variability of NPP model estimates at different scales so the accuracy of NPP estimated at the global scale can also be improved [Ahl *et al.*, 2005]. Consequently, the model validation for NPP estimates and the exploration of the NPP variation related to climate change is very important.

[33] In this study, we used the modeled and estimated NPP (including IGBP and GPPDI) data to compare and validate the simulated global NPP with the two-way coupled model between biosphere and atmosphere. By comparing the spatial pattern of NPP at global and the country-level scale (China, USA and Australia), we found the general consistency of the simulation with IGBP and MODIS data. The global NPP distributions of the model simulations from low, mid to high latitudes were reasonable, compared to the spatial pattern of previous studies [Field *et al.*, 1998; Kicklighter *et al.*, 1999; Running *et al.*, 1999; Bonan *et al.*, 2003; Zeng, 2003]. The underestimated air temperature limiting the vegetation growth in the northern high latitudes leads to the lower simulated NPP. The simulated NPP south of 15°S in Africa is larger than the IGBP and MODIS data and it results from the classification of different ecosystem types; that is, the land cover type is mainly broadleaf trees as the SSiB model [Xue *et al.*, 2004], whereas the shrublands or grasslands are distributed in many other models. The zonal mean NPP values of the simulation in each latitudinal band with 30° interval show the consistency with IGBP and MODIS data except the obviously lower estimate poleward of 60°N.

[34] The country-level NPP was compared and validated using IGBP data, GPPDI data, two global model NPP and ORNL estimate data with the global 0.5° cell. In China, the simulated NPP corresponds well to the IGBP and MODIS data in the spatial pattern with NPP >500 g C m⁻² year⁻¹ south of 35°N in eastern China and up to 700 g C m⁻² year⁻¹ more in southern China, which is reproduced in the new calculation using GloPEM [Cao *et al.*, 2005]. However, in northeast China, the simulated NPP is underestimated (caused by a cold bias) even reaching lower 200 g C m⁻² year⁻¹ north of 48°N compared to IGBP and other modeled and estimated data. By carefully comparing the simulation, IGBP data and GPPDI data north of 48°N in northeast China to previous relevant studies [e.g., Tao *et al.*, 2003; Jiang *et al.*, 1999], we found that the actual NPP in this region may be 350–400 g C m⁻² year⁻¹. The NPP value of Cao *et al.* [2005], MODIS and ORNL data also supports

those values in this area. In the USA, the simulated NPP shows roughly an overall agreement with the IGBP and GPPDI data, but the simulation cannot capture the west-east gradients between 95 and 105°W because the simulated precipitation cannot capture the 1–2.5 mm/day gradient in this area, unlike with CRU data. As a result, along with the north-south gradient impact of air temperature, the west-east NPP band is not shown in the simulation. In Australia, the simulated NPP corresponds to the modeled and estimated data with the large values in the eastern, northern and southwestern belts. The simulated NPP, IGBP and MODIS data in central Australia (200–300 g C m⁻² year⁻¹) reflect the possible underestimate of NPP in GPPDI data (<100 g C m⁻² year⁻¹) depicted in the document from ISLSCP II, but whether or not the NPP value of 200–300 g C m⁻² year⁻¹ is more actual is a decision not to be taken lightly, considering the NPP distribution modeled by Wang and Barrett [2003], which shows less than 200 g C m⁻² year⁻¹ in central Australia.

[35] Every single model simulates the NPP with the discrepancies from other models' result and limited field measurement, which demonstrates again the necessity of model NPP validation against field data at regional and global scales. As for the current data availability, besides field or ground-based measured data, the multimodel ensemble result is another effective and reliable choice for model validation because the ensemble result (e.g., IGBP NPP data in this study) produces better estimates of the real value of NPP than any one particular model taken individually; this is similar to the ensemble results of climate simulations (chapter 9 of the third IPCC report) and surface hydrological simulations [Gordon *et al.*, 2004]. The relative error term (RE) is one quantified criteria to evaluate the model NPP discrepancy against the ensemble result or field data. Compared to IGBP NPP data, the RE values of the coupled model lie around ±20% across the globe and over China, respectively, and more than –30% in the USA and 60% in Australia. This reflects that the best agreement with IGBP data is over the entire globe and China, and the large deviation occurs in the USA and Australia. However, the overall RE values can be compared to those of CASA and GloPEM and are located in the intermediate position at global scale. The area-averaged NPP and correlation coefficients with MODIS data at global and regional scales again reveal that the values of AVIM-GOALS lie generally between the two global models. All the values above show the reasonable overall simulation capacity of the coupled model to capture spatially global and regional NPP in contrast with modeled and estimated NPP.

[36] The response of ecosystem processes at regional and global scales to changing climate is the central theme in the analysis of global change [Tian *et al.*, 1999]. We also compared the globally zonal mean NPP using IGBP data, MODIS data and NPP of two global models and studied the relationship between NPP and climate. The simulated NPP is consistent overall with the NPP data and is lower than IGBP and MODIS data north of 30°N, which is due to the underestimated air temperature (excluding the 30–50°N warm bias of the Tibetan Plateau). In view of the overall latitudinal variation, the global terrestrial NPP corresponds more closely to the precipitation than the air temperature for all NPP data. The month-to-month variation of NPP across

latitudes reflects the seasonal variation of temperature and precipitation, and the seasonal variation in Northern Hemisphere is more obvious than that of the Southern Hemisphere. The global NPP of all data for vegetation types is more strongly correlated to precipitation (higher correlation coefficients at 99.9% significance level) than to temperature, which shows that the climatic effect of moisture is generally the principal limiting factor for global vegetation types. The work of *Lu and Ji* [2006] using AVIM in Northeast China Transect (NECT) presents also the high dependence of moisture including precipitation for spatial distribution of NPP.

[37] To quantify the global and regional NPP is a challenge, however, though it is one useful and reliable way to validate the NPP values with the synthesized NPP as suggested by *Zhao et al.* [2005]. The globally averaged NPP of AVIM-GOALS is $447.47 \text{ g C m}^{-2} \text{ year}^{-1}$ and agrees with the $450.42 \text{ g C m}^{-2} \text{ year}^{-1}$ of IGBP data, but the regional mean NPP is underestimated over China and USA and overestimated over Australia. Global total NPP is meaningful for the global carbon cycle because carbon sinks result from an increase in global terrestrial NPP [*Nemani et al.*, 2003; *Zhao et al.*, 2005]. The simulated global terrestrial total NPP of $53.4 \text{ Pg C year}^{-1}$ is close to the $54.9 \text{ Pg C year}^{-1}$ of IGBP data and it approximates the value of other literature [e.g., *Cao and Woodward*, 1998; *Nemani et al.*, 2003]. The simulated and IGBP data averaged over China are $330.83/417.58 \text{ g C m}^{-2} \text{ year}^{-1}$, whereas other studies [*Xiao et al.*, 1998; *Sun and Zhu*, 2001; *Cao et al.*, 2003, 2005; *He et al.*, 2005] present different values below $400 \text{ g C m}^{-2} \text{ year}^{-1}$. Thus the IGBP value appears to be overestimated to an extent, partly because of the high NPP in northeast China, and the mean value of China below $400 \text{ g C m}^{-2} \text{ year}^{-1}$ may be closer to the truly correct result. Compared to the regional estimate of forest NPP from Resource Planning Act/Forest Inventory and Assessment (RPA/FIA) and CASA model driven with satellite data [*Hicke et al.*, 2002], the NPP of IGBP data averaged over USA seems reasonable with the value of $497.73 \text{ g C m}^{-2} \text{ year}^{-1}$. However, compared to the longer time (1900–1993) mean NPP from the supplementary information of *Nemani et al.* [2002], the IGBP data of USA appear to be about $90 \text{ g C m}^{-2} \text{ year}^{-1}$ high. The ORNL NPP averaged over the USA reveals the higher IGBP data as well. The simulated NPP over the USA in the coupled model AVIM-GOALS is underestimated because of the lower NPP north of 42°N . For the NPP averaged over Australia, it is difficult for us to draw a definite conclusion because the national-level NPP varies considerably, similar to that in the work of *Roxburgh et al.* [2004] (who presented twelve model estimates of long-term annual total NPP ranging from 0.67 to $3.31 \text{ Pg C year}^{-1}$). We make a roughly hypothetical calculation with the ratio of the areas of Australia to global land areas (0.0502) and using the method of *Raupach and Moran* [1998] we found that the global terrestrial total NPP for the simulation and IGBP data multiplied by 0.0502 is 2.68 and $2.76 \text{ Pg C year}^{-1}$, and the two total NPP values of the Australian continent seem to be within the range presented by *Roxburgh et al.* [2004]. On the basis of the analysis above, we can conclude that the global and national-level mean NPP should be validated further in future with more field data as suggested by *Cao et al.*

[2003]. Also, the regional mean NPP shows more uncertainty than the global average.

[38] Generally speaking, the simulated NPP is accurate in the global distribution. However, at a national scale, it shows the regional bias due to the different impacts of climate, such as the underestimate in northeast China caused by cold bias and not reproducing the $95\text{--}105^\circ\text{W}$ west-east gradient in the USA from the spatial weakness of precipitation. Correlation and relative error term (RE) were used to evaluate the simulated NPP at global and regional scale and show the similar spatial strength and weakness of simulation. In contrast with the regional correlation with MODIS data, the coupled model simulates NPP better over China than USA and Australia. This can also be reflected in the RE values of AVIM-GOALS with respect to IGBP data.

[39] IGBP and GPPDI data show the good spatial pattern for the distribution of NPP, even at the national scale. Compared to previous literature and estimated data, IGBP data capture the reasonable NPP magnitude from the regional scale in China, USA and Australia, up to global estimate. Its highest correlation coefficient with MODIS data (0.75 of USA to 0.90 of Australia) in all modeled NPP shows the best reasonable global and regional spatial structure in contrast with the three global models. The relative percentage of maximum, minimum and range for NPP across global vegetation types with respect to MODIS data is between $\pm 15\%$, reflecting the best and smallest variation amplitude in all modeled NPP values. However, the deficiency appears to be the slight overestimate of NPP in northeast China. Compared to data of *Cao et al.* [2005], previous literature, MODIS data and ORNL data, IGBP NPP north of 48°N in northeast China seems to be at least a $50 \text{ g C m}^{-2} \text{ year}^{-1}$ overestimate. For IGBP NPP across global vegetation type, vegetation type 8 affects the correlation with CRU temperature markedly and lowers the correlation coefficient significantly; however the explanation for this effect is complicated and will not be discussed here. GPPDI data obtained from field data exhibit finer distribution at regional scales such as in the USA. The field data can guarantee the high quality of the GPPDI data from the perspective of data source, but the carbon allocation method in central Australia leads to the possible underestimate of approximately $100 \text{ g C m}^{-2} \text{ year}^{-1}$ as described by the ISLSCP II document, and the lower NPP may be true in contrast to that of MODIS data, IGBP data and CASA model.

[40] Admittedly, MODIS data are also not the global observation NPP. However, the NPP estimate from satellite data is potentially accurate for global NPP distribution [*Zhao et al.*, 2006] and can provide good quality data for the validation of model NPP. Thus we can use MODIS NPP as a reference to compare the spatial distribution between all modeled NPP and IGBP data, especially the relationship for global vegetation types. MODIS NPP used in this paper is averaged during 2000–2003, and strictly speaking, the 4-year mean has inconsistency to a degree compared with the multiyear mean NPP of other global models. However, for current global NPP data available, use of MODIS data is a good choice to validate the NPP simulation from global climate-vegetation models, especially in global and regional spatial distributions. This comparison method with insufficient duration is similar to the work of *Zhao et al.* [2006]

using 2- or 3-year mean MODIS NPP from the year of 2000 to compare against EMDI NPP data. On the other hand, considering the increase of NPP in northeast China since the 1980s [Cao *et al.*, 2003, 2005], MODIS data in this region should be higher than NPP in the 1980s. However, MODIS NPP in northeast China is lower than IGBP data and this discrepancy again supports the overestimated IGBP NPP in this region. Global models of GloPEM and CASA with different moisture schemes for NPP controlling may estimate high and low global NPP, respectively [Cramer *et al.*, 1999]. The discussion of the discrepancy in the two models is out of the scope of this study. In other words, the models were just used in a comparison for global and regional NPP simulation in spatial pattern to show the model performance of AVIM-GOALS in contrast with other representative global biogeochemical models.

[41] The coarse resolution of GOALS GCM due to time-consuming calculation exerts some limit on the NPP simulation resulting from the land-sea border control (e.g., in the western coast areas of USA and Australia), but it does not influence much of the study as presented in this paper at global and regional scales. The higher resolution of GCM should be coupled to simulate terrestrial NPP distribution and variation at global/regional scales. Fortunately, the R42 L9 GOALS GCM with the grid approximately 2.815° longitude by 1.67° latitude has been developed and is in progress [Wu *et al.*, 2003], and we think the finer resolution of a two-way coupled model in the future will improve the simulated NPP distribution at the regional scale to an extent, such as the closer capture of spatial heterogeneity in contrast to other model and estimated data, with the finer resolution of AVIM (better for 0.5° by 0.5°).

[42] In fact, the actual global observation of NPP distribution data is still unavailable at present. For instance, the GPPDI data derived from field measured NPP can provide the data for model validation only in some regions such as the three countries in this study (scattered, sparse data in China), and there are no records with 0.5° in many regions of the globe. As a result, the NPP data, which incompletely covers the surface of the globe, causes some limitations on our model validation, and hence the validation should be carried out further with more field data aggregated to the appropriate spatial scale suitable for model validation in the future.

[43] **Acknowledgments.** This work was supported by National Basic Research Program of China “the Development and Application of a Regional Model of the Earth System” (grant 2006CB400506), the Innovation Project of Chinese Academy of Sciences (grant KZCX3-SW-229), and the project of National Natural Science Foundation of China (grant 40205013). J. Ji was funded by NKBRF under grant 2002CB412503. We thank ISLSCP II for providing the CRU data, IGBP data and GPPDI data. We also acknowledge Christopher Michael Brodowski and Liza P. Koshy for the English editing of this paper.

References

- Ahl, D. T., S. T. Gower, D. S. Mackay, S. N. Burrows, J. M. Norman, and G. R. Diak (2005), The effects of aggregated land cover data on estimating NPP in northern Wisconsin, *Remote Sens. Environ.*, *97*, 1–14.
- Bonan, G. B., S. Levis, S. Sitch, M. Vertenstein, and K. W. Oleson (2003), A dynamical global vegetation model for use with climate models: Concepts and description of simulated vegetation dynamics, *Global Change Biol.*, *9*, 1543–1566.
- Cao, M. K., and F. I. Woodward (1998), Net primary and ecosystem production and carbon stocks of terrestrial ecosystems and their responses to climate change, *Global Change Biol.*, *4*, 185–198.
- Cao, M. K., B. Tao, K. R. Li, X. M. Shao, and S. D. Prince (2003), Interannual variation in terrestrial ecosystem carbon fluxes in China from 1981 to 1998, *Acta Bot. Sin.*, *45*, 552–560.
- Cao, M. K., S. D. Prince, B. Tao, J. Small, and K. R. Li (2005), Regional pattern and interannual variations in global terrestrial carbon uptake in response to changes in climate and atmospheric CO₂, *Tellus, Ser. B*, *57*, 210–217.
- Chen, L. J., G. H. Liu, and H. G. Li (2002), Estimating net primary productivity of terrestrial vegetation in China using remote sensing (in Chinese), *J. Remote Sens.*, *6*, 129–135.
- Ciais, P., P. P. Tans, M. Trolier, J. W. C. White, and R. J. Francey (1995), A large Northern Hemisphere terrestrial CO₂ sink indicated by the ¹³C/¹²C ratio of atmospheric CO₂, *Science*, *269*, 1098–1102.
- Clark, D. A., S. Brown, D. W. Kicklighter, J. Q. Chambers, J. R. Thomlinson, J. Ni, and E. A. Holland (2001), Net primary production in tropical forests: An evaluation and synthesis of existing field data, *Ecol. Appl.*, *11*, 371–384.
- Coquard, J., P. B. Buffry, K. E. Taylor, and J. P. Iorio (2004), Present and future surface climate in the western USA as simulated by 15 global climate models, *Clim. Dyn.*, *23*, 455–472.
- Cox, P. M., R. A. Betts, C. D. Jones, S. A. Spall, and L. J. Totterdell (2000), Acceleration of global warming due to carbon-cycle feedbacks in a coupled climate model, *Nature*, *408*, 184–187.
- Cramer, W., D. W. Kicklighter, A. Bondeau, B. Moore, G. Churkina, B. Nemry, A. Ruimy, A. L. Schloss, and the participants of the Potsdam NPP Model Intercomparison (1999), Comparing global models of terrestrial net primary productivity (NPP): Overview and key results, *Global Change Biol.*, *5*, suppl. 1, 1–15.
- Dan, L., J. J. Ji, and Y. P. Li (2005), Climatic and biological simulations in a two-way coupled atmosphere-biosphere model (CABM), *Global Planet. Change*, *47*, 153–169.
- Dorman, J. L., and P. J. Sellers (1989), A global climatology of albedo, roughness length and stomatal resistance for atmospheric general circulation models as represented by the Simple Biosphere Model (SiB), *J. Appl. Meteorol.*, *28*, 833–855.
- Field, C. B., M. J. Behrenfeld, J. T. Randerson, and P. Falkowski (1998), Primary production of the biosphere: Integrating terrestrial and oceanic components, *Science*, *281*, 237–240.
- Foley, J. A., S. Levis, I. C. Prentice, D. Pollard, and S. L. Thompson (1998), Coupling dynamical models of climate and vegetation, *Global Change Biol.*, *4*, 561–579.
- Forestry Ministry of China (1994), *Statistics on Forest Resources of China (1989–1993)* (in Chinese), 385 pp., For. Publ., Beijing, China.
- Goetz, S. J., S. D. Prince, J. Small, and A. C. R. Gleason (2000), Interannual variability of global terrestrial primary production: Results of a model driven with satellite observations, *J. Geophys. Res.*, *105*, 20,077–20,091.
- Gordon, W. S., J. S. Famiglietti, N. L. Fowler, T. G. F. Kittel, and K. A. Hibbarde (2004), Validation of simulated runoff from six terrestrial ecosystem models: Results from VEMAP, *Ecol. Appl.*, *14*, 527–545.
- Haywood, J. M., R. J. Stouffer, R. T. Wetherald, S. Manabe, and V. Ramanaswamy (1997), Transient response of a coupled model to estimated changes in greenhouse gas and sulphate concentrations, *Geophys. Res. Lett.*, *24*, 1335–1338.
- He, Y., L. Dan, W. J. Dong, J. J. Ji, and D. H. Qin (2005), The terrestrial NPP simulations in China since Last Glacial Maximum, *Chin. Sci. Bull.*, *50*, 2074–2079.
- Hicke, J. A., G. P. Asner, J. T. Randerson, C. Tucker, S. Los, R. Birdsey, J. C. Jenkins, C. Field, and E. Holland (2002), Satellite-derived increases in net primary productivity across North America, 1982–1998, *Geophys. Res. Lett.*, *29*(10), 1427, doi:10.1029/2001GL013578.
- Houghton, J. T., Y. Ding, D. J. Griggs, M. Noguer, P. J. van der Linden, and D. Xiaosu (Eds.) (2001), Model evaluation, in *Climate Change 2001: The Scientific Basis—Contribution of Working Group I to the Third Assessment Report of the Intergovernmental Panel on Climate Change*, pp. 471–523, Cambridge Univ. Press, New York.
- Hunt, E. R., S. C. Piper, R. Nemani, C. D. Keeling, R. D. Otto, and S. W. Running (1996), Global net carbon exchange and intra-annual atmospheric CO₂ concentrations predicted by an ecosystem process model and three-dimensional atmospheric transport model, *Global Biogeochem. Cycles*, *10*, 431–456.
- Ji, J. J. (1995), A climate-vegetation interaction model: Simulating physical and biological processes at the surface, *J. Biogeogr.*, *22*, 445–451.
- Ji, J. J., and Y. C. Hu (1989), A simple land surface process model for use in climate studies, *Acta Meteorol. Sin.*, *3*, 344–353.
- Ji, J. J., and L. Yu (1999), A simulation study of coupled feedback mechanism between physical and biogeochemical processes at the surface (in Chinese), *Chin. J. Atmos. Sci.*, *23*, 439–448.
- Jiang, H., M. J. Apps, Y. L. Zhang, C. H. Peng, and P. M. Woodare (1999), Modelling the spatial pattern of net primary productivity in Chinese forests, *Ecol. Modell.*, *122*, 275–288.

- Ju, L. X., and H. J. Wang (2006), A regional climate model nested in a global gridpoint general circulation model, *Chin. J. Geophys.*, *49*, 49–58.
- Kicklighter, D. W., A. Donbeau, A. L. Schloss, J. Kaduk, A. D. McGuire, and the participants of the Potsdam NPP Model Intercomparison (1999), Comparing global models of terrestrial net primary productivity (NPP): Global pattern and differentiation by major biomes, *Global Change Biol.*, *5*, suppl. 1, 16–24.
- Lau, N. C., and M. J. Nath (2004), Coupled GCM simulation of atmosphere-ocean variability associated with zonally asymmetric SST changes in the tropical Indian Ocean, *J. Clim.*, *17*, 245–265.
- Li, Y. P., and J. J. Ji (2001), Model estimates of global carbon flux between vegetation and the atmosphere, *Adv. Atmos. Sci.*, *18*, 807–818.
- Liu, Y. M., G. X. Wu, H. Liu, and P. Liu (2001), Condensation heating of the Asian summer monsoon and the subtropical anticyclone in the Eastern Hemisphere, *Clim. Dyn.*, *19*, 327–338.
- Liu, Y. M., G. X. Wu, and R. C. Ren (2004), Relationship between the subtropical anticyclone and diabatic heating, *J. Clim.*, *17*, 682–698.
- Lu, J. H., and J. J. Ji (2002), A simulation study of atmosphere-vegetation interactions over the Tibetan Plateau, part II: Net primary productivity and leaf area index (in Chinese), *Chin. J. Atmos. Sci.*, *26*, 254–262.
- Lu, J. H., and J. J. Ji (2006), A simulation and mechanism analysis of long-term variations at land surface over arid/semi-arid area in north China, *J. Geophys. Res.*, *111*, D09306, doi:10.1029/2005JD006252.
- Nemani, R., M. White, P. Thornton, K. Nishida, S. Reddy, J. Jenkins, and S. Running (2002), Recent trends in hydrologic balance have enhanced the terrestrial carbon sink in the United States, *Geophys. Res. Lett.*, *29*(10), 1468, doi:10.1029/2002GL014867.
- Nemani, R. R., C. D. Keeling, H. Hashimoto, W. M. Jolly, S. C. Piper, C. J. Tucker, R. B. Myneni, and S. W. Running (2003), Climate-driven increases in global terrestrial net primary production from 1982 to 1999, *Science*, *300*, 1560–1563.
- New, M., M. Hulme, and P. Jones (1999), Representing twentieth-century space-time climate variability. Part I: Development of a 1961–90 mean monthly terrestrial climatology, *J. Clim.*, *12*, 829–856.
- Olson, R. J., K. Johnson, D. Zheng, and J. M. O. Scurlock (2001), Global and regional ecosystem modeling: Databases of model drivers and validation measurements, *ORNL/TM-2001/196*, 84 pp., Environ. Sci. Div., Oak Ridge Natl. Lab., Oak Ridge, Tenn.
- Phillips, N. A. (1973), Principles of large scale numerical weather prediction, in *Dynamic Meteorology*, edited by P. Morel, pp. 3–96, Springer, New York.
- Potter, C. S. (1999), Terrestrial biomass and the effects of deforestation on the global carbon cycle, *Bioscience*, *49*, 769–778.
- Potter, C. S., S. A. Klooster, R. Myneni, V. Genovese, P.-N. Tan, and V. Kumar (2003), Continental-scale comparisons of terrestrial carbon sinks estimated from satellite data and ecosystem modeling 1982–1998, *Global Planet. Change*, *39*, 201–213.
- Prince, S., and J. Small (2003), AVHRR Global Production Efficiency Model, 1981–2000, Global Land Cover Facil., College Park, Md.
- Raich, J. W., and K. J. Nadelhoffer (1989), Belowground carbon allocation in forest ecosystems; global trends, *Ecology*, *70*, 1346–1354.
- Raupach, M. R., and C. Moran (1998), Material budgets as an organising framework: Contributions to methods development for the national and water resources audit, *Tech. Rep. 27/98*, 23 pp., CSIRO Land and Water, Canberra, A. C. T., Australia.
- Roxburgh, S. H., et al. (2004), A critical overview of model estimates of net primary productivity for the Australian continent, *Functional Plant Biol.*, *31*, 1043–1059.
- Ruimy, A., L. Kergoat, A. Bondeau, and the participants of the Potsdam NPP Model Intercomparison (1999), Comparing global models of terrestrial net primary productivity (NPP): Analysis of differences in light absorption and light-use efficiency, *Global Change Biol.*, *5*, suppl. 1, 56–64.
- Running, S. W., and E. R. Hunt (1993), Generalization of a forest ecosystem process model for other biomes, BIOME-BGC, and an application for global-scale models, in *Scaling Physiological Processes: Leaf to Globe*, pp. 141–158, edited by J. R. Ehleringer and C. Field, Elsevier, New York.
- Running, S. W., D. D. Baldocchi, D. P. Turner, S. T. Gower, P. S. Bakwin, and K. A. Hibbard (1999), A global terrestrial monitoring network integrating tower fluxes, flask sampling, ecosystem modeling and EOS satellite data, *Remote Sens. Environ.*, *70*, 108–127.
- Scurlock, J. M. O., and R. J. Olson (2002), Terrestrial net primary productivity—A brief history and new worldwide database, *Environ. Rev.*, *10*, 91–109.
- Scurlock, J. M. O., W. Cramer, R. J. Olson, W. J. Parton, and S. D. Prince (1999), Terrestrial NPP: Towards a consistent data set for global model evaluation, *Ecol. Appl.*, *9*, 913–919.
- Sun, R., and Q. J. Zhu (2001), Estimation of net primary productivity in China using remote sensing data, *J. Geogr. Sci.*, *11*, 14–23.
- Tao, B., K. R. Li, X. M. Shao, and M. K. Cao (2003), Temporal and spatial pattern of net primary production of terrestrial ecosystems in China (in Chinese), *Acta Geogr. Sin.*, *58*, 372–380.
- Tian, H., J. M. Melillo, D. W. Kicklighter, A. D. McGuire, and J. Helfrich (1999), The sensitivity of terrestrial carbon storage to historical climate variability and atmospheric CO₂ in the United States, *Tellus, Ser. B*, *51*, 414–452.
- Wang, B., H. Liu, and G. Y. Shi (2000), Radiation and cloud scheme, in *IAP Global Ocean Atmosphere-Land System Model*, edited by X. H. Zhang et al., chap. 3, pp. 28–49, Sci. Press, Beijing.
- Wang, S. Q., C. H. Zhou, J. Y. Liu, K. R. Li, and X. M. Yang (2001), Simulation analyses of terrestrial carbon cycle balance model in northeast China (in Chinese), *Acta Geogr. Sin.*, *56*, 390–400.
- Wang, Y., L. A. Mysak, and N. T. Roulet (2005), Holocene climate and carbon cycle dynamics: experiments with the “green” McGill Paleoclimate Model, *Global Biogeochem. Cycles*, *19*, GB3022, doi:10.1029/2005GB002484.
- Wang, Y. P., and D. J. Barrett (2003), Estimating regional terrestrial carbon fluxes for the Australian continent using a multiple-constraint approach, part I: Using remotely sensed data and ecological observations of net primary production, *Tellus, Ser. B*, *55*, 270–289.
- Williams, J. W., E. W. Seabloom, D. Slayback, D. M. Stoms, and J. H. Viers (2005), Anthropogenic impacts upon plant species richness and net primary productivity in California, *Ecol. Lett.*, *8*, 127–137.
- Wu, G. X., H. Liu, Y. C. Zhao, and W. P. Li (1996), A nine-layer atmospheric general circulation model and its performance, *Adv. Atmos. Sci.*, *13*, 1–18.
- Wu, G. X., X. H. Zhang, H. Liu, Y. Q. Yu, X. Z. Jin, Y. F. Guo, S. F. Sun, W. P. Li, B. Wang, and G. Y. Shi (1997), Global ocean-atmosphere-land system model of LASG (GOALS/LASG) and its performance in simulation study (in Chinese), *Q. J. Appl. Meteorol.*, *8*, 15–28.
- Wu, T. W., P. Liu, Z. Z. Wang, Y. M. Liu, R. C. Yu, and G. X. Wu (2003), The performance of atmospheric component model R42L9 of GOALS/LASG, *Adv. Atmos. Sci.*, *20*, 726–742.
- Xiao, X. M., J. M. Melillo, D. W. Kicklighter, Y. Pan, A. D. McGuire, and J. Helfrich (1998), Net primary production of terrestrial ecosystems in China and its equilibrium responses to changes in climate and atmospheric CO₂ concentration, *Acta Phytoecol. Sin.*, *22*, 97–118.
- Xue, Y., H. M. H. Juang, W. P. Li, S. Prince, R. DeFries, Y. Jiao, and R. Vasic (2004), Role of land surface processes in monsoon development: East Asia and West Africa, *J. Geophys. Res.*, *109*, D03105, doi:10.1029/2003JD003556.
- Zeng, N. (2003), Glacial-interglacial atmospheric CO₂ change—the glacial burial hypothesis, *Adv. Atmos. Sci.*, *20*, 677–693.
- Zeng, Q. C. (1963), Characteristic parameters and dynamical equations of atmospheric motions (in Chinese), *Acta Meteorol. Sin.*, *33*, 472–498.
- Zhang, T., G. X. Wu, and Y. F. Guo (2002), Energy budget bias in global coupled ocean-atmosphere-land model (in Chinese), *Acta Meteorol. Sin.*, *60*, 278–289.
- Zhao, M. S., F. A. Heinsch, R. R. Nemani, and S. W. Running (2005), Improvements of the MODIS terrestrial gross and net primary production global data set, *Remote Sens. Environ.*, *95*, 164–176.
- Zhao, M. S., S. W. Running, and R. R. Nemani (2006), Sensitivity of Moderate Resolution Imaging Spectroradiometer (MODIS) terrestrial primary production to the accuracy of meteorological reanalyses, *J. Geophys. Res.*, *111*, G01002, doi:10.1029/2004JG000004.
- Zheng, D. L., S. Prince, and R. Wright (2003), Terrestrial net primary production estimates for 0.5° grid cells from field observations—A contribution to global biogeochemical modeling, *Global Change Biol.*, *9*, 46–64.
- Zheng, D. L., S. D. Prince, and R. Wright (2004), NPP multi-biome: Gridded estimates for selected regions worldwide, 1989–2001, revision 2, <http://www.daac.ornl.gov>, Oak Ridge Natl. Lab. Distrib. Active Arch. Cent., Oak Ridge, Tenn.
- Zhou, G. S., and X. S. Zhang (1995), A natural vegetation NPP model (in Chinese), *Acta Phytoecol. Sin.*, *19*, 193–200.
- Zhou, T. J., and Y. F. Qian (1995), The design and forecast verification of an one-way nested fine-mesh limited area numerical model (in Chinese), *J. Trop. Meteorol.*, *11*, 342–353.
- Zobler, L. (1986), A world soil file for global climate modeling, *NASA Tech. Memo. 87802*, 33 pp.

L. Dan and J. Ji, START Regional Center for Temperate East Asia and Key Laboratory of Regional Climate-Environment for Temperate East Asia, Institute of Atmospheric Physics, Chinese Academy of Sciences, Beijing 100029, China. (danli@tea.ac.cn)

Y. He, National Climate Center, China Meteorological Administration, Beijing 100081, China.